729 Lw ~~4892~~

ORNL-4892

FINAL REPORT ON A BENCHMARK EXPERIMENT FOR NEUTRON TRANSPORT THROUGH IRON AND STAINLESS STEEL

R. E. Maerker
F. J. Muckenthaler

BLANK PAGE

Printed in the United States of America. Available from
National Technical Information Service
U.S. Department of Commerce
5285 Port Royal Road, Springfield, Virginia 22151
Price: Printed Copy $5.45; Microfiche $1.45

ORNL-4892
UC-79d - Liquid Metal Fast
Breeder Reactors Physics

Contract No. W-7405-eng-26

Neutron Physics Division

FINAL REPORT ON A BENCHMARK EXPERIMENT FOR NEUTRON TRANSPORT THROUGH IRON AND STAINLESS STEEL

R. E. Maerker and F. J. Muckenthaler

APRIL 1974

OAK RIDGE NATIONAL LABORATORY
Oak Ridge, Tennessee 37830
operated by
UNION CARBIDE CORPORATION
for the
U. S. ATOMIC ENERGY COMMISSION

TABLE OF CONTENTS

Abstract

An experiment concerning neutron penetration in iron and stainless steel is described, and experimental results are presented which provide a basis for verification of the accuracy of iron cross sections to be used in transport calculations. The experiment was performed at the Tower Shielding Facility of ORNL and included measurements of both the neutron fluence and neutron spectra through samples of iron up to 3 ft thick and of stainless steel up to 18 in. thick. Calculations of the experiment were performed with a special version of the MORSE multigroup Monte Carlo code which uses point total cross sections. Comparison of the calculations with experiment indicates that the recently evaluated MAT 4180-Mod. 1 iron cross-section set is superior to the older MAT 1101 and MAT 1124 sets. Calculations using this newest set result in total neutron leakages above thermal energies penetrating up to 3 ft of iron or 18 in. of stainless steel that agree with experiment to within about 20%. The calculated leakage spectra above 90 keV arising from scattering through up to 1 ft of iron or 18 in. of stainless steel also agree with experiment to within about 20%. Using any of the three sets, the calculated unscattered component through 1 ft of iron or stainless steel above 1 MeV is only accurate to within about 40%.

INTRODUCTION

Both the top shield and the structural components in the design of the FTR contain a large amount of iron in the form of carbon and stainless steels, and the iron therefore constitutes an important part of the neutron shield. The carbon steels consist of relatively pure iron, while the stainless steels contain considerable amounts of chromium and nickel. Since these steel components have thicknesses of the order of 3 ft, it is essential that accurate experimental results be available to verify transport calculations for deep penetration of neutrons through iron. Results from earlier experiments,[1] which were conducted for this purpose, have been somewhat limited in usefulness because of the relatively small iron thicknesses. The present experimental results were compared with calculations performed using a special version of the MORSE multigroup Monte Carlo code employing point total cross sections. The comparisons of the calculated results with experimental results for several spectrometers and integral detectors having widely varying energy responses have been utilized to determine the accuracy of the transport calculations using the latest available cross-section sets. Through sensitivity analysis, these results can be used to predict the dose uncertainty in a calculation for an LMFBR shield.

DESCRIPTION OF THE EXPERIMENT

A series of deep-penetration neutron transmission measurements through iron slabs up to 3 ft thick and stainless steel slabs up to 18 in. thick have been performed at the Tower Shielding Facility (TSF) using a collimated beam of reactor neutrons as a source. These measurements were made behind

BLANK PAGE

various combinations of 5-ft-sq slabs; therefore, because the beam was tightly collimated, the effects of side leakage even for the 3-ft-thick sample of iron were negligible. Figure 1 shows a schematic of the experimental geometry for the thickest sample.

The thickness, density, and composition of the individual slabs used in the experiment were accurately determined. The density of the Type-304 stainless steel slabs averaged 7.86 grams/cm^3 and that of the iron slabs averaged 7.79 grams/cm^3. The average composition of the slabs is shown in Table I, where it is to be observed that the "iron" slabs were actually carbon steel.

Detailed measurements of the transmitted neutron spectra were made behind 1 ft of iron and 18 in. of stainless steel, covering the energy range from ~80 keV to 10 MeV, using two types of spectrometers. These were (1) an NE-213 scintillator, which determines spectra in the energy range 0.8 to 15 MeV with the aid of the unfolding code FERDOR;[2,3] and (2) a Benjamin proton recoil spectrometer which determines spectra in the range ~ 80 keV to 1.5 MeV with the aid of the unfolding code SPEC4.[4] In addition, a ^{10}B spectrometer[5] which determines the spectra in the range thermal to ~ 10 keV with the aid of an iterative folding procedure was used behind 0.5 and 1.5 in. of iron. A set of three spherical BF_3 detectors surrounded by various thicknesses of polyethylene (0.5 to 4 in.) and an outside shell of cadmium were also used to obtain weighted integral flux measurements behind thicknesses of iron varying from 1.5 in. to 3 ft and of stainless steel from 1 to 1.5 ft. These "Bonner ball" detectors have response functions which peak in different regions of the neutron spectrum. A description of each Bonner ball is given in Table II. The response function of each

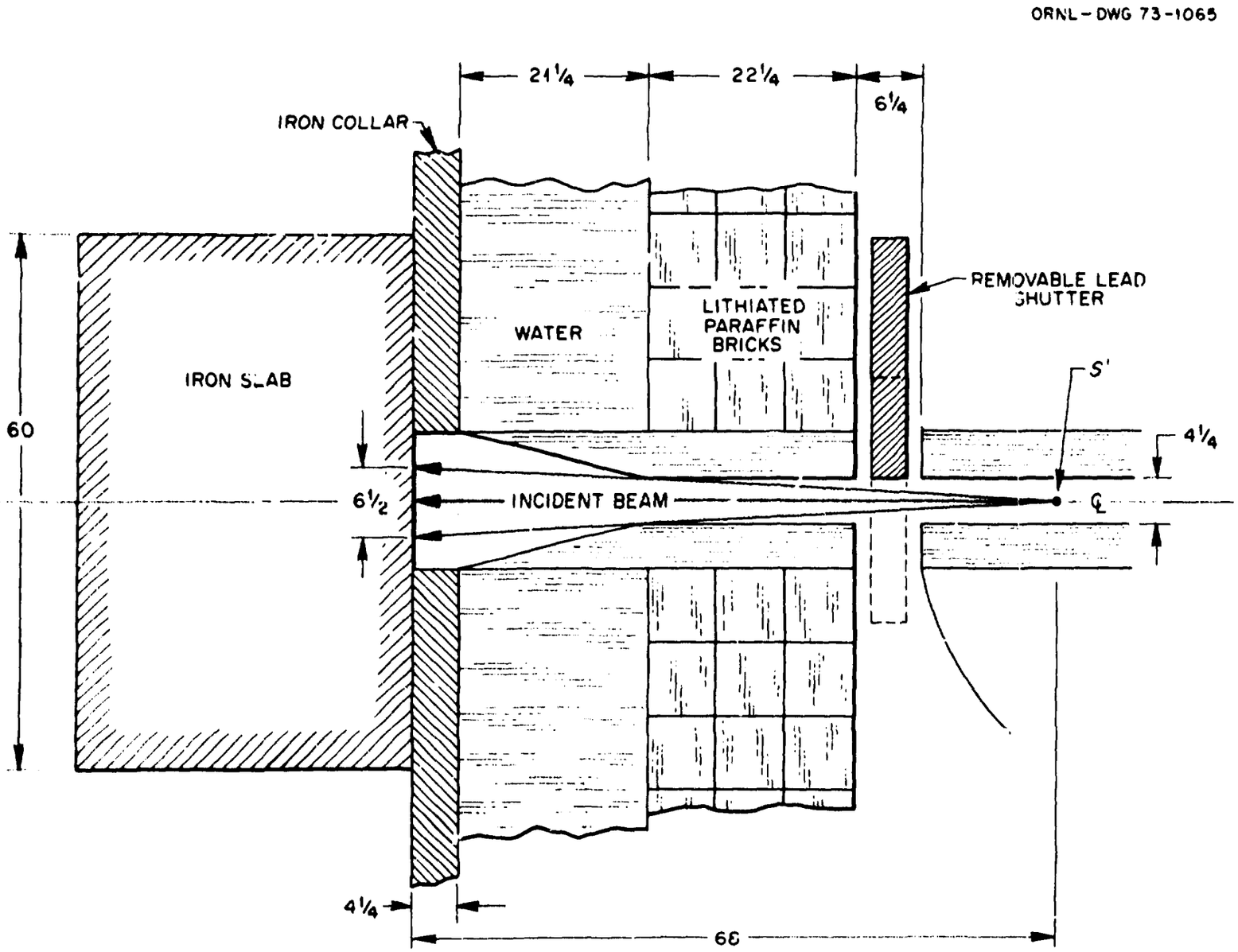

Fig. 1. Experimental Configuration for the 4-1/4-in.-diam Collimator with the 3-ft-thick Iron Slab in Place. This collimator was used for all the measurements except those made behind 18 in. of stainless steel.

Table I. Composition of the Slabs in Atoms/barn-cm

	Iron Slabs	Stainless Steel Slabs
Carbon	9.815×10^{-4}	-
Manganese	5.150×10^{-4}	1.14×10^{-3}
Iron	8.372×10^{-2}	5.995×10^{-2}
Chromium	-	1.686×10^{-2}
Nickel	-	7.90×10^{-3}

Bonner ball was determined[6,7] as a function of energy to within a few percent utilizing ANISN adjoint calculations and calibrations with known sources. It is expressed in units of counts/second per neutron/cm^2/sec of energy E uniformly incident over the outside hemispherical surface of the ball.

Because of the importance of determining the characteristics of the neutron source for this experiment, measurements of the incident neutron beam were made with each of the three spectrometers. This provided a measured absolute energy spectrum from thermal to 10 MeV. The angular distribution of the source was also measured using several detectors by mapping of the beam in both the transverse and axial directions. These measurements established the fact that the tightly collimated source could be represented as a virtual point anisotropic source located 68 in. inside the collimator from the edge of the iron collar (point S' in Fig. 1), with the beam intensity uniform over a diameter of ~6-1/2 in. at the mouth of the collimator and zero elsewhere.

The absolute source spectrum determined from the spectrometer measurements for the centerline point located on the exit plane of the collimator is shown in Fig. 2 for the region 100 eV $\leq$ E $\leq$ 10 MeV, and tabulated in Table III for a 220-group structure to facilitate transport calculations in iron. The accuracy of the absolute magnitude of the incident spectrum is estimated to be $\pm$ 10% down to 200 keV and $\pm$ 20% below 200 keV. The energy resolution varies from 30% at 1 MeV to about 10% at 10 MeV. Below 1 MeV, the resolution is constant at about 10% down to 100 keV. The ratio of surface-integrated current over the collimator to centerline current is 212.5 cm^2.

Table II. Bonner Ball Description
Spherical, 2-in.-diam $^{10}BF_3$ Proportional Counter Surrounded by Polyethylene and 0.030-in. Cd

Standard Bonner Ball Designation	Polyethylene Thickness (in.)	Polyethylene Density (grams/cm^3)	Diameter of Ball (in.)	Displacement of Center of Detection from Geometric Center (in.)*
3	0.515	0.951	3.09	0.9
6	1.91	0.925	5.88	1.8
10	3.90	0.951	9.86	3.0

*The direction of this displacement is toward the center of gravity of the hemispherical surface upon which the neutrons are incident.

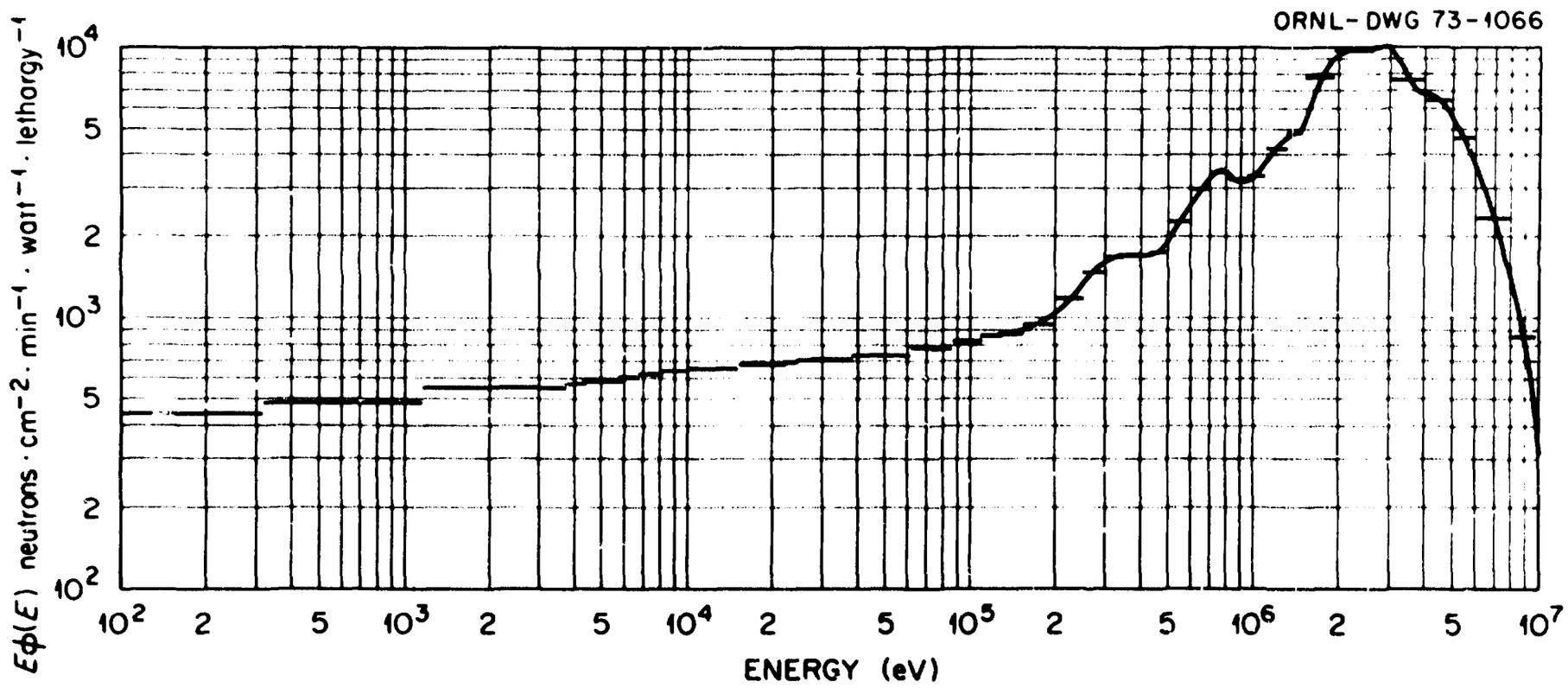

Fig. 2. Neutron Beam Source Spectrum on the Centerline at the Outside Edge of the 4-1/4-in.-diam Collimator.

Table III. Source Spectrum at the Edge of the Iron Collar Shown in Fig. 1 in Neutrons/cm^2/min/W/Group

Group	Energy Interval	Intensity	Group	Energy Interval	Intensity
1	8–10 MeV	190	31	1.405–1.411 MeV	23.8
2	6–8	665	32	1.401–1.405	16.6
3	5–6	840	33	1.392–1.401	35.4
4	4–5	1426	34	1.382–1.392	40.1
5	3–4	2186	35	1.363–1.382	74.5
6	2.59–3	1479	36	1.339–1.363	93.5
7	2.38–2.59	887	37	1.313–1.339	98.2
8	2.35–2.38	130	38	1.306–1.313	25.9
9	2.262–2.35	384	39	1.291–1.306	56.8
10	2.232–2.262	130	40	1.285–1.291	22.5
11	1.943–2.232	1267	41	1.251–1.285	125
12	1.90–1.943	190	42	1.244–1.251	25.9
13	1.889–1.90	47.5	43	1.221–1.244	84.5
14	1.82–1.889	301	44	1.217–1.221	14.2
15	1.81–1.82	43.8	45	1.211–1.217	21.3
16	1.783–1.81	118	46	1.205–1.211	21.2
17	1.747–1.783	153	47	1.197–1.205	28.4
18	1.722–1.747	109	48	1.192–1.197	17.7
19	1.686–1.722	153	49	1.169–1.192	79.2
20	1.680–1.686	25.9	50	1.155–1.169	48.6
21	1.6465–1.680	143	51	1.136–1.155	65.0
22	1.638–1.6465	39.1	52	1.130–1.136	20.1
23	1.587–1.638	219	53	1.1195–1.130	34.3
24	1.567–1.587	85.0	54	1.1165–1.1195	10.0
25	1.522–1.567	190	55	1.1135–1.1165	10.0
26	1.506–1.522	67.6	56	1.107–1.1135	23.8
27	1.497–1.506	38.0	57	1.098–1.107	29.6
28	1.472–1.497	104	58	1.090–1.098	26.0
29	1.442–1.472	125	59	1.084–1.090	20.1
30	1.411–1.442	124	60	1.029–1.084	177

Table III. (Cont'd.)

Group	Energy Interval	Intensity	Group	Energy Interval	Intensity
61	1.023-1.029 MeV	20.1	93	769-820 keV	216
62	1.020-1.023	10.0	94	767-769	8.98
63	1.013-1.020	23.8	95	752.5-767	67.6
64	0.998-1.013	49.6	96	751-752.5	6.85
65	992-998 keV	19.5	97	741-751	47.5
66	982-992	32.8	98	739-741	9.49
67	974-982	26.4	99	732-739	33.8
68	960-974	46.5	100	710-732	107
69	957-960	10.0	101	700-710	48.6
70	951-957	20.1	102	697-700	14.8
71	946-951	16.9	103	693-697	19.5
72	944-946	6.85	104	691-693	9.49
73	941.5-944	8.44	105	663-691	134
74	939.5-941.5	6.85	106	659-663	19.0
75	936-939.5	12.1	107	652.5-659	30.6
76	932-936	13.7	108	648-652.5	21.1
77	927-932	17.4	109	644-648	18.5
78	919-927	28.0	110	638-644	28.0
79	917-919	7.39	111	620-638	82.9
80	898.5-917	65.5	112	616.5-620	15.8
81	891-898.5	27.5	113	612 5-616.5	18.0
82	882-891	33.3	114	607.5-612.5	22.2
83	878-882	14.8	115	590.5-607.5	75.5
84	855.5-878	85.5	116	580-590.5	45.9
85	852.5-855.5	11.6	117	576-580	16.9
86	846.5-852.5	23.2	118	569.6-576	27.5
87	839-846.5	29.6	119	560.5-569.5	38.0
88	836-839	12.1	120	559-560.5	6.34
89	834-836	7.93	121	557.5-559	6.34
90	830-834	15.8	122	552.5-557.5	21.1
91	825-830	20.1	123	546.5-552.5	24.8
92	820-825	20.6	124	543-546.5	14.2

Table III. (Cont'd.)

Group	Energy Interval	Intensity	Group	Energy Interval	Intensity
125	5'0-543 keV	12.7	157	267-271	21.9
126	536-540	16.4	158	262-267	27.5
127	534-536	8.12	159	244.8-262	94.7
128	515-534	77.1	160	244-244.8	4.41
129	510.5-515	18.0	161	243.2-244	4.41
130	503-510.5	29.6	162	232-243.2	61.8
131	498-503	19.5	163	219.8-232	65.5
132	493-498	19.0	164	218.6-219.8	6.34
133	469.1-493	90.6	165	208-218.6	56.0
134	467.5-469.1	5.99	166	200-208	42.2
135	464-467.5	13.2	167	185.2-200	78.2
136	437.7-464	99.2	168	182-185.2	16.8
137	436.5-437.7	4.52	169	175-182	36.4
138	433-436.5	13.5	170	168.5-175	34.5
139	378-433	229	171	167.5-168.5	5.38
140	377.2-378	3.73	172	164-167.5	18.9
141	375-377.2	10.2	173	155-164	49.6
142	373.5-375	6.98	174	144-155	63.9
143	359.3-373.5	68.3	175	139.5-144	27.4
144	358.8-359.3	2.42	176	138.3-139.5	7.45
145	357.8-358.8	4.81	177	136.2-138.3	13.3
146	357.5-357.8	2.39	178	134-136.2	14.0
147	354.5-357.3	13.8	179	130-134	26.1
148	350.5-354.5	20.1	180	129.2-130	5.29
149	348.2-350.5	11.5	181	127.5-129.2	11.3
150	331.4-348.2	85.4	182	110-127.5	127
151	330.7-331.4	3.66	183	87-110	193
152	314-330.7	87.3	184	83-87	37.1
153	309.5-314	23.7	185	82.7-83	2.85
154	300-309.5	50.2	186	82.4-82.7	2.85
155	275-300	135	187	81.4-82.4	9.49
156	271-275	21.9	188	80-81.4	13.3

Table III. (Cont'd.)

Group	Energy Interval	Intensity	Group	Energy Interval	Intensity
189	77-80 keV	29.2	207	6.7-8.2	126
190	72-77	51.0	208	5.8-6.7	87.6
191	68-72	44.1	209	4.3-5.8	174
192	62-68	72.4	210	3.7-4.3	86.6
193	38-62	354	211	1.16-3.7	640
194	31-38	143	212	1.14-1.16	8.98
195	27-31	97.4	213	0.3167-1.14	616
196	25.7-27	34.3	214	88-316.7 eV	565
197	25.2-25.7	13.7	215	28.4-88	554
198	24.5-25.2	19.9	216	6.79-24.4	554
199	23.75-24.5	21.5	217	1.89-6.79	555
200	23.25-23.75	14.8	218	0.524-1.89	576
201	22-23.25	38.3	219	0.145-0.524	1542
202	19-22	100	220	0-0.145	6580
203	15-19	158	Totals		
204	10-15	264	1-220	0-10 MeV	3.186×10^4
205	8.8-10	81.3			
206	8.2-8.8	44.3			

A summary of all the detector locations behind the iron and stainless steel slabs is shown in Tables IV and V, respectively. The Bonner ball locations are measured to the geometric center of each ball. Note that all of the measurements behind 18 in. of stainless steel were made using the reactor collimator shown in Fig. 3. For this collimator, the absolute spectrum for point A in Fig. 3 is approximately 7.4 times the spectrum shown in Table III, with the virtual source located 59.5 in. inside the collimator. This source is presented in a 100-group structure in Table VI, and can be readily interpolated to any other structure, such as the 220-group structure appearing in Table III. The ratio of surface-integrated current over the collimator to centerline current is 1200 cm^2 (Ref. 8). The 3- and 6-in. Bonner balls used behind the 18 in. of stainless steel were also slightly different from those described in Table II. The 3-in. ball had a polyethylene thickness of 0.47 in. and the 6-in. ball a polyethylene thickness of 1.97 in., both of density 0.951 grams/cm^3.

The effects of any transverse leakage combined with subsequent air and ground scattering were quantitatively measured for each foreground measurement by placing a thick hydrogenous shield about halfway between the detector and the back face of the slabs in such a way that neutrons leaking from the back face of the slabs could not reach the detector. These background measurements were subtracted from all the foreground measurements (i.e., measurements obtained in the absence of the hydrogenous shadow shield). It should be mentioned that the backgrounds so obtained are underestimates of the true background because of the neglect of subsequent air and ground scattering into the detector of neutrons stopped with the background shield, since the detectors, except for the ^{10}B spectrometer, have no collimator.

Table IV. Experimental Configurations for the Iron Transmission Measurements

Iron Slab Thickness (in.)	Detector Locations: Centerline Distance Behind Slab (in.)	Detector Locations: Radial Distance From Centerline (in.)	Detector Locations: Observation Angle[a] With Respect to Centerline (deg)	Detector Type
0.52	127	0	0	^{10}B Spectrometer
	123	33	15	
	90	90	45	
1.55	152	0	0	Bonner Balls
	146	39	15	
	107	107	45	
	126	0	0	^{10}B Spectrometer
	122	32.5	15	
	89	89	45	
4.05	158	42.5	15	NE-213 Spectrometer
	116	116	45	
6.06	162	0	0	NE-213 Spectrometer
12.13	141	0	0	Bonner Balls
	136	36.5	15	
	100	100	45	
	156	0	0	NE-213 Spectrometer
	150	40.5	15	
	110	110	45	
12.25	10	0	0	Benjamin Spectrometer
	10	12	50	
24.41	128	0	0	Bonner Balls
	124	33	15	
	90.5	90.5	45	
36.56	115	0	0	Bonner Balls
	111	30	15	
	81.5	81.5	45	

[a]The observation angle is defined as the angle between the centerline and a line connecting the detector and the midpoint of the emergent face of the slab. The vertex of this angle is the pivot point for the angular traverses.

Table V. Experimental Configurations for the Stainless Steel Transmission Measurements

Stainless Steel Slab Thickness (in.)	Detector Locations			Detector Type
	Centerline Distance Behind Slab (in.)	Radial Distance From Centerline (in.)	Observation Angle[a] With Respect to Centerline (deg)	
12.17	141	0	0	Bonner Balls
	136	36.5	15	
	100	100	45	
	10	0	0	Benjamin Spectrometer
	10	12	50	
18-33[b]	12 → 140	0	0	Bonner Balls
	47.7	0	0	NE-213 Spectrometer
	12	0	0	Benjamin Spectrometer

[a]The observation angle is defined as the angle between the centerline and a line connecting the detector with the midpoint of the emergent face of the slab. The vertex of this angle is the pivot point for the angular traverses.

[b]All measurements behind 18 in. of stainless steel were made using the collimator described in Fig. 3. The 3-in. and 6-in. Bonner balls were also of slightly different dimensions than those described in Table II. See text.

ORNL-DWG 72-7405R2

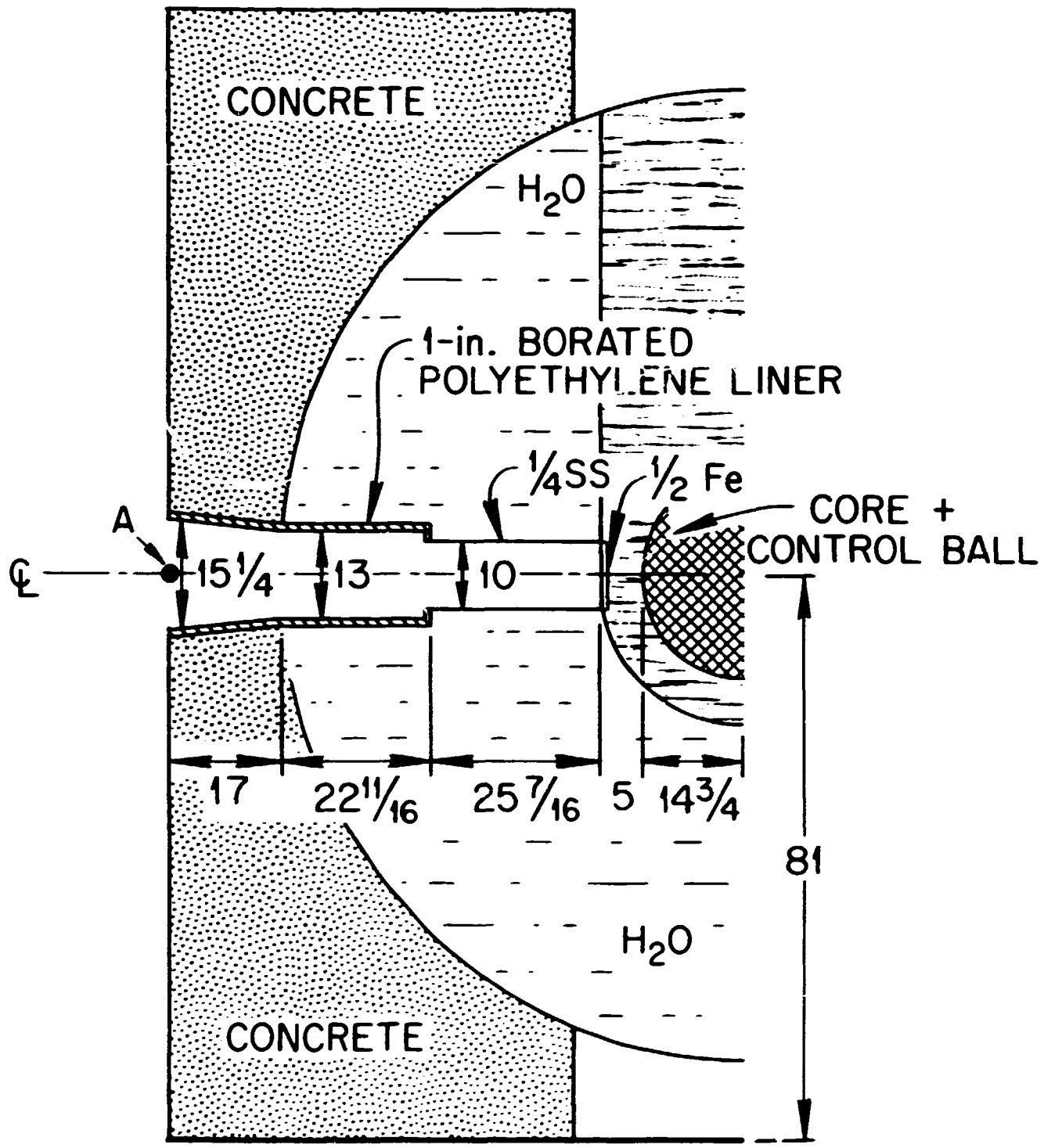

Fig. 3. Experimentai Configuration for the 15-1/4-in.-diam Collimator Used for the Measurements Made Behind 18 in. of Stainless Steel Only.

Table VI. Source Spectrum at Point A in Fig. 3 for the 15-1/4-in. Collimator in Neutrons/cm^2/min/W/Group

Group	Energy Interval	Intensity	Group	Energy Interval	Intensity
1	13.5-14.9 MeV	14	24	1.35-1.50	4000
2	12.2-13.5	32	25	1.22-1.35	3170
3	11.05-12.2	73	26	1.11-1.22	2485
4	10.0-11.05	199	27	1.00-1.11	2350
5	9.04-10.0	312	28	0.907-1.00	2135
6	8.19-9.04	545	29	0.821-0.907	2215
7	7.41-8.19	846	30	0.743-0.821	2345
8	6.70-7.41	1375	31	0.672-0.743	2320
9	6.07-6.70	2070	32	0.608-0.672	1990
10	5.49-6.07	2585	33	0.550-0.608	1700
11	4.97-5.49	3180	34	0.497-0.550	1425
12	4.49-4.97	3665	35	0.450-0.497	1210
13	4.07-4.49	4420	36	0.408-0.450	1130
14	3.68-4.07	4880	37	0.369-0.408	1170
15	3.33-3.68	4825	38	0.334-0.369	1175
16	3.01-3.33	5315	39	0.302-0.334	1130
17	2.73-3.01	6570	40	0.273-0.302	1055
18	2.47-2.73	7075	41	0.247-0.273	955
19	2.23-2.47	6955	42	0.224-0.247	837
20	2.02-2.23	6190	43	0.202-0.224	777
21	1.83-2.02	5570	44	0.183-0.202	926
22	1.65-1.83	5175	45	0.166-0.183	845
23	1.50-1.65	4200	46	0.150-0.166	827

Table VI. (Cont'd.)

Group	Energy Interval	Intensity	Group	Energy Interval	Intensity
47	0.136-0.150 MeV	785	70	583-749	1010
48	0.123-0.136	798	71	454-583	990
49	0.111-0.123	799	72	354-454	970
50	86.5-111 keV	1870	73	275-354	960
51	67.4-86.5	1790	74	214-275	940
52	52.5-67.4	1730	75	167-214	920
53	40.9-52.5	1650	76	130-167	900
54	31.8-40.9	1590	77	101-130	900
55	24.8-31.8	1530	78	78.9-101	900
56	19.3-24.8	1490	79	61.4-78.9	900
57	15.0-19.3	1440	80	47.9-61.4	900
58	11.7-15.0	1370	81	37.3-47.9	900
59	9.12-11.7	1340	82	29.0-37.3	900
60	7.10-9.12	1310	83	22.6-29.0	900
61	5.53-7.10	1260	84	17.6-22.6	900
62	4.31-5.53	1220	85	13.7-17.6	900
63	3.35-4.31	1200	86	10.7-13.7	930
64	2.61-3.35	1180	87	8.32-10.7	960
65	2.03-2.61	1150	88	6.48-8.32	990
66	1.58-2.03	1120	89	5.04-6.48	1035
67	1.23-1.58	1100	90	3.93-5.04	1035
68	961-1230 eV	1030	91	3.06-3.93	1035
69	749-961	1020	92	2.38-3.06	1035

Table VI. (Cont'd.)

Group	Energy Interval	Intensity
93	1.86-2.38	1060
94	1.44-1.86	1100
95	1.13-1.44	1170
96	0.876-1.13	1250
97	0.683-0.876	1350
98	0.532-0.683	1565
99	0.414-0.532	1900
100	0.000-0.414	9.50×10^4
Totals 1-100	0.000-14.9 MeV	2.702×10^5

TABULATED RESULTS OF THE MEASUREMENTS BEHIND THE SLABS

All the measurements have an estimated reproducibility of ±5%, due primarily to power calibration uncertainties.

The results of unfolding the ^{10}B spectrometer measurements behind 1/2 in. of iron are shown in Table VII. The unfolded spectra produced calculated counting rates that agreed with the measured counting rates behind all the filters within 10% on the average.

Table VII. Measured Low Energy Spectra Behind 1/2 in. of Iron

Energy	Intensity			Energy	Intensity		
(eV)	Centerline	15°	45°	(eV)	Centerline	15°	45°
	$\phi(E)$, neutrons/cm^2/min/W				$E\phi(E)$, neutrons/cm^2/min/W/U		
Thermal	212	1.53	0.862	40	9.92	0.0854	0.0484
	$E\phi(E)$, neutrons/cm^2/min/W/U			50	9.92	0.0854	0.0484
0.4	33.2	0.238	0.135	60	9.92	0.0854	0.0484
0.5	28.2	0.206	0.117	70	9.92	0.0854	0.0484
0.6	24.4	0.180	0.101	80	9.92	0.0854	0.0484
0.7	21.9	0.161	0.0914	90	9.92	0.0854	0.0484
0.8	19.8	0.152	0.0863	100	9.92	0.0854	0.0484
0.9	18.8	0.145	0.0822	200	9.92	0.0854	0.0484
1	17.7	0.141	0.0802	300	9.92	0.0854	0.0484
2	13.7	0.119	0.0676	400	9.92	0.0854	0.0484
3	12.8	0.111	0.0629	500	9.92	0.0854	0.0484
4	12.1	0.106	0.0596	600	9.92	0.0854	0.0484
5	11.6	0.102	0.0576	700	9.92	0.0854	0.0484
6	11.3	0.0996	0.0564	800	11.2	0.0854	0.0484
7	11.2	0.0980	0.0556	900	12.3	0.0854	0.0484
8	11.1	0.0960	0.0545	1000	13.3	0.0854	0.0484
9	11.0	0.0945	0.0536	2000	23.3	0.0854	0.0484
10	10.8	0.0923	0.0523	3000	32.3	0.0854	0.0484
20	10.4	0.0900	0.0511	4000	40.8	0.0854	0.0484
30	10.1	0.0867	0.0491				

The results of unfolding the ^{10}B spectrometer measurements behind 1-1/2 in. of iron are shown in Table VIII. The unfolded spectra produced calculated counting rates that agreed with the measured counting rates behind all the filters within an averaged 10% for the centerline and 15° cases and 20% for the 45° case.

Table VIII. Measured Low-Energy Spectra Behind 1-1/2 in. of Iron

Energy	Intensity			Energy	Intensity		
(eV)	Center-line	15°	45°	(eV)	Center-line	15°	45°
	$\phi(E)$, neutrons/cm^2/min/W				$E\phi(E)$, neutrons/cm^2/min/W/U		
Thermal	14.2	0.453	0.283	40	0.429	0.0661	0.0531
	$E\phi(E)$, neutrons/cm^2/min/W/U			50	0.429	0.0661	0.0531
0.4	2.40	0.0792	0.0634	60	0.429	0.0661	0.0531
0.5	2.14	0.0792	0.0634	70	0.429	0.0661	0.0531
0.6	1.93	0.0792	0.0634	80	0.429	0.0661	0.0531
0.7	1.76	0.0792	0.0634	90	0.429	0.0661	0.0531
0.8	1.65	0.0792	0.0634	100	0.429	0.0661	0.0531
0.9	1.55	0.0792	0.0634	200	0.429	0.0661	0.0531
1	1.46	0.0792	0.0634	300	0.429	0.0661	0.0531
2	1.00	0.0792	0.0634	400	0.429	0.0661	0.0531
3	0.816	0.0792	0.0634	500	0.429	0.0661	0.0531
4	0.707	0.0792	0.0634	600	0.429	0.0661	0.0531
5	0.624	0.0792	0.0634	700	0.429	0.0661	0.0531
6	0.429	0.0772	0.0618	800	0.429	0.0661	0.0531
7	0.429	0.0760	0.0608	900	0.429	0.0661	0.0531
8	0.429	0.0746	0.0598	1000	0.429	0.0661	0.0531
9	0.429	0.0737	0.0589	2000	0.858	0.0661	0.0531
10	0.429	0.0716	0.0573	3000	1.29	0.0661	0.0531
20	0.429	0.0702	0.0562	4000	1.72	0.0661	0.0531
30	0.429	0.0676	0.0540	5000	2.15	0.0661	0.0531

The measured Bonner ball counting rates behind the iron slabs are shown in Tables IX-XII, where the 3.09-in.- and 5.88-in.-diam Bonner balls were used along with the collimator described in Fig. 1 and Table III.

Table IX. Measured Bonner Ball Counting Rates Behind 1-1/2 in. of Iron in Counts/Min/W

Bonner Ball	3-in.			6-in.			10-in.		
	CL	15°	45°	CL	15°	45°	CL	15°	45°
Foreground	58.44	1.607	1.079	609.1	6.903	3.855	587.7	5.675	2.503
Background	0.67	0.587	0.399	1.7	1.685	1.033	0.9	0.938	0.517
Net	57.8	1.02	0.680	607	5.22	2.82	587	4.75	1.99

Table X. Measured Bonner Ball Counting Rates Behind 12 in. of Iron in Counts/Min/W

Bonner Ball	3-in.			6-in.			10-in.		
	CL	15°	45°	CL	15°	45°	CL	15°	45°
Foreground	2.667	0.9041	0.6612	19.325	4.347	3.018	10.186	1.869	1.247
Background	0.349	0.3271	0.2503	0.866	0.813	0.626	0.301	0.285	0.213
Net	2.32	0.577	0.411	18.5	3.53	2.39	9.89	1.58	1.03

Table XI. Measured Bonner Ball Counting Rates Behind 24 in. of Iron in Counts/Min/W

Bonner Ball	3-in.			6-in.			10-in.		
	CL	15°	45°	CL	15°	45°	CL	15°	45°
Foreground	0.8039	0.5474	0.3999	3.921	2.085	1.456	1.519	0.7047	0.4909
Background	0.1996	0.180†	0.1549	0.435	0.385†	0.327	0.120	0.105†	0.0862
Net	0.604	0.367	0.245	3.49	1.70	1.13	1.40	0.600	0.405

† Interpolated values.

Table XII. Measured Bonner Ball Counting Rates
Behind 36 in. of Iron in Counts/Min/W

Bonner Ball	3-in.			6-in.			10-in.		
	CL	15°	45°	CL	15°	45°	CL	15°	45°
Foreground	0.3573	0.2878	0.2203	1.298	0.9023	0.6488	0.4255	0.2787	0.1961
Background	0.1146	0.107†	0.0929	0.218	0.202†	0.1743	0.0572	0.052†	0.0451
Net	0.243	0.181	0.127	1.08	0.700	0.475	0.368	0.227	0.151

†Interpolated values.

The measured Bonner ball counting rates behind 12 in. of stainless steel using the collimator described in Fig. 1 and Table III appear in Table XIII and behind 18 in. of stainless steel using the collimator described in Fig. 3 and Table VI appear in Tables XIV - XVI. The 3-in. and 6-in. Bonner balls used in the measurements presented in Table XIII are the same 3.09-in.- and 5.88-in.-diam balls used for the measurements behind iron.

Table XIII. Measured Bonner Ball Counting Rates
Behind 12 in. of Stainless Steel in Counts/Min/W

Bonner Ball	3-in.			6-in.			10-in.		
	CL	15°	45°	CL	15°	45°	CL	15°	45°
Foreground	1.0954	0.7829	0.5470	6.757	3.473	2.334	3.779	1.524	0.9841
Background	0.3122	0.2866	0.2201	0.790	0.729	0.560	0.271	0.247	0.1872
Net	0.783	0.496	0.327	5.97	2.74	1.77	3.51	1.28	0.797

Table XIV. Measured 3-in.† Bonner Ball Counting Rates
Along an Axial Traverse Behind 18 in. of Stainless Steel in Counts/Min/W

CL Distance Behind Slab (in.)	12	24	48	72	96	120	140
Foreground	432.6	214.2	81.85	40.88	25.38	17.26	13.107
Background	4.950††	4.839††	4.558††	4.278	3.998††	3.717††	3.437
Net	428	209	77.3	36.6	21.4	13.5	9.67

†The 3.00-in. diam Bonner ball.

††Interpolated values.

Table XV. Measured 6-in.† Bonner Ball Counting Rates Along an Axial Traverse Behind 18 in. of Stainless Steel in Counts/Min/W

CL Distance Behind Slab (in.)	12	24	36	48	72	96	120	140
Foreground	2516	1239	707.8	452.9	230.4	139.3	94.48	70.34
Background	14.40††	14.12††	13.77††	13.42††	12.67	12.00††	11.30††	10.52
Net	2502	1225	694	439	218	127	83.2	59.8

†The 6.00 in.-diam Bonner ball.

††Interpolated values.

Table XVI. Measured 10-in. Bonner Ball Counting Rates Along an Axial Traverse Behind 18 in. of Stainless Steel in Counts/Min/W

CL Distance Behind Slab (in.)	12	24	48	72	96	120	140
Foreground	1012	476.4	173.9	87.08	51.70	34.69	25.26
Background	3.620†	3.564†	3.414†	3.264	3.114†	2.964†	2.814
Net	1008	473	170	83.8	48.6	31.7	22.4

†Interpolated values.

The tabulated unfolded Benjamin spectrometer data obtained behind the 12-in. slabs appear in Tables XVII-XX. The standard error pertains to counting statistics only.

The tabulated unfolded Benjamin spectrometer data obtained behind the 18-in. stainless steel slab using the 15-1/4-in. collimator appear in Table XXI. Again, the standard error pertains to counting statistics only.

Table XVII. Unfolded Benjamin Counter Spectrum on the Centerline 10 in. Behind 12 in. of Iron

Energy Interval (keV)	Flux (neutrons/cm^2/MeV/min/W)	Std. Error (%)
	10 Atmosphere Counter	
1379.3-1500	20.4	9.6
1277.1-1379.3	32.3	7.4
1184.2-1277.1	46.4	5.8
1091.3-1184.2	52.4	5.2
1017.0-1091.3	52.4	6.7
933.4-1017.0	65.7	4.6
868.4-933.4	59.2	6.6
803.4-868.4	54.8	6.8
738.4-803.4	91.6	3.9
682.7-738.4	158	2.7
636.2-682.7	195	2.7
589.8-636.2	182	2.9
	3 Atmosphere Counter	
644.7-700	228	3.5
597.9-644.7	233	4.2
551.1-597.9	133	7.0
512.8-551.1	108	10.4
474.5-512.8	118	8.8
436.2-474.5	98.7	9.7
406.4-436.2	129	9.2
372.3-406.4	233	4.1
346.8-372.3	309	4.1
321.3-346.8	351	3.5
295.7-321.3	372	3.1
274.5-295.7	340	4.0
253.2-274.5	254	5.0
236.2-253.2	220	6.8
214.9-236.2	180	6.0

Table XVII. (Cont'd.)

Energy Interval (keV)	Flux (neutrons/cm^2/MeV/min/W)	Std. Error (%)
	1 Atmosphere Counter	
275.5-300	380	4.0
255.4-275.5	291	6.3
237.5-255.4	215	9.2
219.7-237.5	204	8.9
201.9-219.7	179	9.2
186.2-201.9	273	5.5
172.9-186.2	384	5.1
159.5-172.9	312	5.9
148.3-159.5	334	6.2
137.2-148.3	592	3.3
126.0-137.2	528	3.5
117.1-126.0	317	6.8
108.2-117.1	192	10.3
99.3-108.2	129	14.0
92.6-99.3	156	14.0
85.9-92.6	222	9.1
79.2-85.9	253	7.4
72.5-79.2	242	7.1
68.0-72.5	257	8.7
63.6-68.0	163	12.8
59.1-63.6	210	9.2

Table XVIII. Unfolded Benjamin Counter Spectrum
12 in. off the Centerline and 10 in. Behind 12 in. of Iron

Energy Interval (keV)	Flux (neutrons/cm^2/MeV/min/W)	Std. Error (%)
	10 Atmosphere Counter	
1379.3-1500	4.97	12.0
1277.1-1379.3	6.81	10.6
1184.2-1277.1	10.3	7.9
1091.3-1184.2	12.4	6.6
1017.0-1091.3	14.7	7.4
933.4-1017.0	18.6	5.0
868.4-933.4	21.4	5.9
803.4-868.4	20.7	6.0
738.4-803.4	20.7	6.0
738.4-803.4	31.3	3.9
682.7-738.4	52.7	2.8
636.2-682.7	74.8	2.5
589.8-636.2	72.4	2.6
	3 Atmosphere Counter	
645.0-700	69.2	4.4
598.5-645.0	95.8	4.0
552.0-598.5	70.0	5.5
509.7-552.0	54.5	7.6
471.6-509.7	60.8	7.3
437.8-471.6	54.3	8.8
403.9-347.8	51.6	8.6
374.3-403.9	95.4	5.2
344.7-374.3	131	3.6
319.3-344.7	157	3.5
294.0-319.3	167	3.1
272.8-294.0	152	4.1
251.7-272.8	133	4.4
234.7-251.7	120	5.8
217.8-234.7	97.4	6.7

Table XVIII. (Cont'd.)

Energy Interval (keV)	Flux (neutrons/cm^2/MeV/min/W)	Std. Error (%)
	1 Atmosphere Counter	
275.6-300	165	5.7
255.7-275.6	147	7.8
235.8-255.7	119	9.0
218.1-235.8	107	10.7
202.6-218.1	83.2	14.9
187.1-202.6	130	8.8
173.8-187.1	175	7.3
160.5-173.8	164	7.3
147.2-160.5	159	6.9
136.2-147.2	273	4.6
127.3-136.2	268	5.7
116.2-127.3	189	6.0
107.4-116.2	119	11.0
100.7-107.4	81.3	19.7
91.9-100.7	80.9	13.7
85.2-91.9	113	11.8
78.6-85.2	149	8.4
74.2-78.6	148	11.1
67.5-74.2	182	6.0
63.1-67.5	141	10.1
58.7-63.1	120	11.1

Table XIX. Unfolded Benjamin Counter Spectrum on the Centerline 10 in. Behind 12 in. of Stainless Steel

Energy Interval (keV)	Flux (neutrons/cm^2/MeV/min/W)	Std. Error (%)
	10 Atmosphere Counter	
1379.3-1500	14.0	7.4
1277.1-1379.3	19.6	6.4
1184.2-1277.1	28.2	5.0
1091.3-1184.2	32.4	4.3
1017.0-1091.3	36.2	5.0
933.4-1017.0	41.5	3.7
868.4-933.4	40.6	5.0
803.4-868.4	42.8	4.5
738.4-803.4	61.2	3.0
682.7-738.4	88.1	2.5
636.2-682.7	102	2.6
589.8-636.2	112	2.3
543.3-589.8	101	2.5
506.2-543.3	88.9	3.4
459.8-506.2	90.4	2.5
431.9-459.8	102	3.5
394-431.9	124	2.1
366.9-394.7	145	2.2
339.0-366.9	166	1.9
	3 Atmosphere Counter	
552.3-600	109	6.0
513.4-552.3	87.0	9.3
474.4-513.4	84.7	9.0
439.7-474.4	72.4	11.2
405.1-439.7	83.6	9.0
374.7-405.1	140	5.9
344.4-374.7	166	4.7
318.4-344.4	233	3.8
296.8-318.4	243	4.3

Table XIX. (Cont'd.)

Energy Interval (keV)	Flux (neutrons/cm^2/MeV/min/W)	Std. Error (%)
275.1-296.8	254	4.0
253.4-275.1	193	5.0
236.1-253.4	163	7.0
218.8-236.1	137	7.7
201.4-218.8	128	7.6
184.1-201.4	153	5.9
171.1-184.1	148	7.4
158.1-171.1	131	7.7
145.1-158.1	223	4.2
	1 Atmosphere Counter	
230.0-250	173	7.4
212.2-230.0	146	9.4
196.7-212.2	120	12.3
181.1-196.7	190	7.2
167.8-181.1	202	7.4
156.7-167.8	168	10.2
143.3-156.7	254	5.1
134.4-143.3	440	4.3
123.3-134.4	412	3.5
114.4-123.3	270	6.2
105.6-114.4	158	9.8
96.7-105.6	136	10.5
90.0-96.7	182	9.5
83.3-90.0	239	6.7
76.7-83.3	261	5.7
72.2-76.7	211	9.3
65.6-72.2	217	6.0
61.1-65.6	221	7.7
56.7-61.1	197	8.0

Table XX. Benjamin Counter Spectrum 12 in. Off the Centerline and 10 in. Behind 12 in. of Stainless Steel

Energy Interval (keV)	Flux (neutrons/cm^2/MeV/min/W)	Std. Error (%)
	10 Atmosphere Counter	
1380-1500	3.74	14.4
1278.5-1380	5.93	11.1
1186.2-1278.5	7.92	9.3
1093.8-1186.2	10.9	6.9
1010.8-1093.8	13.7	6.3
936.9-1010.8	15.1	6.6
863.1-936.9	16.1	6.1
798.5-863.1	18.4	6.1
743.1-798.5	22.8	5.8
687.7-743.1	36.5	3.6
632.3-687.7	49.4	2.7
586.2-632.3	53.7	3.0
540.0-586.2	50.6	3.2
503.1-540.0	48.1	4.1
466.2-503.1	46.2	4.1
429.2-466.2	49.3	3.7
401.5-429.2	59.8	3.8
364.6-401.5	75.9	2.2
336.9-364.6	89.6	2.4
	3 Atmosphere Counter	
359.4-400	86.8	4.5
338.8-369.4	93.1	4.0
316.9-338.8	133	4.0
290.7-316.9	129	3.3
268.9-290.7	128	3.9
251.4-268.9	102	5.8
229.5-251.4	81.4	5.4
212.0-229.5	75.9	6.8
198.9-212.0	81.5	7.8

Table XX. (Cont'd.)

Energy Interval (keV)	Flux (neutrons/cm^2/MeV/min/W)	Std. Error (%)
181.4-198.9	93.7	4.8
168.3-181.4	86.5	6.4
155.2-168.3	96.1	5.3
146.4-155.2	162	4.2
	1 Atmosphere Counter	
230.0-250	112	8.1
212.2-230.0	88.9	10.9
196.7-212.2	73.5	14.3
181.1-196.7	100	9.7
167.8-181.1	114	9.4
156.7-167.8	98.7	12.4
143.3-156.7	147	6.3
134.4-143.3	244	5.6
123.3-134.4	240	4.3
114.4-123.3	182	6.7
105.6-114.4	107	10.6
96.7-105.6	70.5	14.7
90.0-96.7	100	12.6
83.3-90.0	150	7.8
76.7-83.3	174	6.3
72.2-76.7	166	8.8
65.6-72.2	158	6.1
61.1-65.6	146	8.6
56.7-61.1	145	8.1

Table XXI. Unfolded Benjamin Counter Spectrum on the Centerline 12 in. Behind 18 in. of Stainless Steel

Energy Interval (keV)	Flux (neutrons/cm^2/MeV/min/W)	Std. Error (%)
	10 Atmosphere Counter	
1169.5-1300.0	78.8	4.9
1048.4-1169.5	121	3.8
945.9-1048.4	179	3.4
852.7-945.9	210	3.3
768.8-852.7	251	3.2
684.9-768.3	469	1.7
619.7-684.9	775	1.5
554.5-619.7	925	1.3
	3 Atmosphere Counter	
630.2-700.0	671	1.9
564.8-630.2	960	1.5
508.1-564.8	832	2.1
455.8-508.1	797	2.3
412.1-455.8	788	2.7
372.9-412.1	1440	1.6
333.6-372.9	2123	1.1
298.8-333.6	2858	0.9
268.2-298.8	3094	1.0
242.1-268.2	2302	1.4
220.2-242.1	2158	1.8
198.4-220.2	2078	1.7
	1 Atmosphere Counter	
225.1-250.0	2405	3.2
202.0-225.1	2072	3.8
182.4-202.0	2394	3.7
162.8-182.4	2888	2.8
146.8-162.8	2922	3.3
132.6-146.8	5612	1.8

Table XXI. (Cont'd.)

Energy Interval (keV)	Flux (neutrons/cm^2/MeV/min/W)	Std. Error (%)
118.3-132.6	5668	1.7
107.7-118.3	3680	3.4
97.0-107.7	2568	4.5
86.3-97.0	4010	2.6
77.4-86.3	5513	2.1
70.3-77.4	4893	2.8
63.2-70.3	4205	3.0
57.8-63.2	3673	4.2
50.7-57.8	3319	3.2
45.4-50.7	4008	3.1
41.8-45.4	3528	4.6
38.3-41.8	2716	5.5

The unfolded NE-213 spectral data behind the iron slabs appear in Tables XXII-XXVII. The limits of the spectrum at each energy are due to combined statistical and unfolding uncertainties.

Table XXII. Unfolded NE-213 Spectrum 15 Deg Off the Centerline Behind 4 in. of Iron

Energy (MeV)	Flux (neutrons/cm^2/MeV/min/W)	
	Upper Limit	Lower Limit
0.8	1.11	1.03
0.9	1.04	0.97
1.0	0.98	0.92
1.1	0.92	0.86
1.2	0.82	0.78
1.3	0.74	0.70
1.4	0.68	0.64
1.5	0.65	0.61
1.6	0.62	0.58
1.7	0.57	0.54
1.8	0.52	0.48
1.0	0.48	0.45
2.0	0.46	0.44
2.1	0.46	0.43
2.2	0.45	0.43
2.3	0.44	0.41
2.4	0.43	0.41
2.5	0.41	0.39
2.6	0.40	0.38
2.7	0.37	0.36
2.8	0.345	0.305
3.0	0.285	0.272
3.2	0.235	0.22
3.4	0.20	0.19

Table XXII. (Cont'd.)

Energy (MeV)	Flux (neutrons/cm^2/MeV/min/W) Upper Limit	Lower Limit
3.6	0.185	0.175
3.8	0.185	0.175
4.0	0.185	0.175
4.2	0.177	0.167
4.4	0.158	0.150
4.6	0.140	0.132
4.8	0.128	0.120
5.0	0.120	0.113
5.2	0.107	0.100
5.4	0.092	0.085
5.6	0.082	0.076
5.8	0.079	0.073
6.0	0.076	0.070
6.2	0.070	0.064
6.4	0.064	0.059
6.6	0.060	0.0545
6.8	0.0535	0.049
7.0	0.045	0.041
7.2	0.037	0.033
7.4	0.032	0.028
7.6	0.0283	0.0248
7.8	0.026	0.0225
8.0	0.0232	0.020
8.2	0.020	0.0173
8.4	0.0177	0.015
8.6	0.016	0.0133
8.8	0.0144	0.0119
9.0	0.013	0.010
9.2	0.0117	0.0094
9.4	0.0107	0.0086
9.6	0.0100	0.0080

Table XXII. (Cont'd.)

Energy (MeV)	Flux (neutrons/cm²/MeV/min/W) Upper Limit	Lower Limit
9.8	0.0094	0.0076
10.0	0.0086	0.0069
10.2	0.0077	0.0060
10.4	0.0067	0.0052
10.6	0.0057	0.0043
10.8	0.0046	0.0032
11.0	0.0033	0.0019

Table XXIII. Unfolded NE-213 Spectrum 45 Deg Off the Centerline Behind 4 in. of Iron

Energy (MeV)	Flux (neutrons/cm^2/MeV/min/W) Upper Limit	Lower Limit
0.8	0.876	0.753
0.9	0.813	0.677
1.0	0.720	0.638
1.1	0.632	0.575
1.2	0.546	0.499
1.3	0.492	0.454
1.4	0.435	0.401
1.5	0.376	0.343
1.6	0.337	0.309
1.7	0.314	0.290
1.8	0.292	0.269
1.9	0.255	0.237
2.0	0.225	0.208
2.1	0.212	0.197
2.2	0.203	0.189
2.3	0.192	0.181
2.4	0.186	0.175
2.5	0.175	0.165
2.6	0.154	0.145
2.7	0.134	0.126
2.8	0.123	0.115
2.9	0.116	0.108
3.0	0.108	0.100
3.2	0.0843	0.0772
3.4	0.0669	0.0596
3.6	0.0580	0.0508
3.8	0.0543	0.0468
4.0	0.0491	0.0421
4.2	0.0480	0.0420
4.4	0.0486	0.0432

Table XXIII. (Cont'd.)

Energy (MeV)	Flux (neutrons/cm^2/MeV/min/W) Upper Limit	Lower Limit
4.6	0.0400	0.0350
4.8	0.0296	0.0252
5.0	0.0252	0.0210
5.2	0.0244	0.0203
5.4	0.0225	0.0189
5.6	0.0190	0.0156
5.8	0.0153	0.0121
6.0	0.0145	0.0114
6.2	0.0140	0.0111
6.4	0.0124	0.00962
6.6	0.0104	0.00780
6.8	0.00931	0.00703
7.0	0.00856	0.00650
7.2	0.00674	0.00464
7.4	0.00564	0.00376
7.6	0.00582	0.00414
7.8	0.00501	0.00334
8.0	0.00312	0.00163
8.2	0.00226	0.00098
8.4	0.00233	0.00109
8.6	0.00223	0.00108
8.8	0.00235	0.00130
9.0	0.00271	0.00172
9.2	0.00256	0.00163
9.4	0.00190	0.00098
9.6	0.00133	0.00052
9.8	0.00113	0.00039
10.0	0.00100	0.00023
10.2	0.00080	0.00005
10.4	0.00075	0.00001
10.6	0.00082	0.00006
10.8	0.00079	0.00006

Table XXIV. Unfolded NE-213 Spectrum on the Centerline Behind 6 in. of Iron

Energy (MeV)	Flux (neutrons/cm^2/MeV/min/W) Upper Limit	Lower Limit
0.8	24.7	22.9
0.9	23.6	21.8
1.0	22.6	21.3
1.1	22.1	21.0
1.2	21.0	20.2
1.3	19.0	18.3
1.4	17.1	16.3
1.5	15.5	14.8
1.6	14.3	13.8
1.7	13.4	12.9
1.8	12.2	11.7
1.9	11.0	10.4
2.0	9.8	9.4
2.1	9.0	8.6
2.2	8.2	7.9
2.3	7.5	7.3
2.4	6.85	6.6
2.5	6.2	6.0
2.6	5.65	5.55
2.7	5.15	5.0
2.8	4.65	4.55
2.9	4.2	4.1
3.0	3.8	3.7
3.2	2.97	2.86
3.4	2.32	2.23
3.6	1.90	1.82
3.8	1.60	1.55
4.0	1.45	1.38
4.2	1.30	1.25
4.4	1.18	1.14
4.6	1.07	1.03
4.8	0.945	0.90

Table XXIV. (Cont'd.)

Energy (MeV)	Flux (neutrons/cm^2/MeV/min/W) Upper Limit	Lower Limit
5.0	0.82	0.74
5.2	0.68	0.64
5.4	0.605	0.57
5.6	0.56	0.52
5.8	0.52	0.485
6.0	0.49	0.455
6.2	0.44	0.415
6.4	0.39	0.36
6.6	0.345	0.32
6.8	0.325	0.297
7.0	0.300	0.275
7.2	0.268	0.243
7.4	0.222	0.200
7.6	0.190	0.170
7.8	0.175	0.155
8.0	0.165	0.147
8.2	0.154	0.137
8.4	0.143	0.126
8.6	0.134	0.117
8.8	0.124	0.108
9.0	0.113	0.098
9.2	0.104	0.089
9.4	0.095	0.080
9.6	0.084	0.070
9.8	0.071	0.058
10.0	0.060	0.047
10.2	0.050	0.038
10.4	0.042	0.031
10.6	0.039	0.028
10.8	0.041	0.029
11.0	0.044	0.033
11.2	0.046	0.035

Table XXV. Unfolded NE-213 Spectrum on the Centerline Behind 12 in. of Iron

Energy (MeV)	Flux (neutrons/cm^2/MeV/min/W) Upper Limit	Lower Limit
0.8	4.8	4.6
0.9	4.2	4.0
1.0	3.9	3.8
1.1	3.65	3.55
1.2	3.35	3.25
1.3	2.7	2.6
1.4	2.1	2.0
1.5	1.65	1.55
1.6	1.35	1.3
1.7	1.12	1.08
1.8	0.94	0.92
1.9	0.78	0.76
2.0	0.66	0.64
2.1	0.54	0.52
2.2	0.46	0.44
2.3	0.38	0.37
2.4	0.315	0.305
2.5	0.255	0.250
2.6	0.210	0.205
2.7	0.170	0.165
2.8	0.143	0.138
2.9	0.119	0.115
3.0	0.097	0.094
3.2	0.068	0.065
3.4	0.050	0.046
3.6	0.037	0.035
3.8	0.030	0.027
4.0	0.027	0.024
4.2	0.0245	0.0220
4.4	0.0205	0.0180
4.6	0.017	0.015
4.8	0.014	0.012

Table XXV. (Cont'd.)

Energy (MeV)	Flux (neutrons/cm^2/MeV/min/W) Upper Limit	Lower Limit
5.0	0.0123	0.0105
5.2	0.0117	0.0097
5.4	0.0109	0.0091
5.6	0.0096	0.0080
5.8	0.0080	0.0065
6.0	0.0075	0.0060
6.2	0.0068	0.0052
6.4	0.0063	0.0046
6.6	0.0060	0.0043
6.8	0.0058	0.0042
7.0	0.0054	0.0040
7.2	0.0051	0.0038
7.4	0.0051	0.0037
7.6	0.0050	0.0037
7.8	0.0044	0.0032
8.0	0.0039	0.0028
8.2	0.0038	0.0026
8.4	0.0036	0.0025
8.6	0.0033	0.0022
8.8	0.0027	0.0017
9.0	0.0025	0.0014
9.2	0.0026	0.0016
9.4	0.0028	0.0018
9.6	0.0028	0.0018
9.8	0.0026	0.0016
10.0	0.0023	0.0013
10.2	0.0022	0.0012
10.4	0.0021	0.0013
10.6	0.0021	0.0013
10.8	0.0020	0.0011

Table XXVI. Unfolded NE-213 Spectrum 15 Deg Off the Centerline Behind 12 in. of Iron

Energy (MeV)	Flux (neutrons/cm^2/MeV/min/W) Upper Limit	Lower Limit
0.8	0.50	0.49
0.9	0.39	0.38
1.0	0.31	0.30
1.1	0.250	0.245
1.2	0.21	0.20
1.3	0.165	0.160
1.4	0.140	0.135
1.5	0.115	0.110
1.6	0.095	0.092
1.7	0.079	0.077
1.8	0.068	0.065
1.9	0.058	0.055
2.0	0.050	0.046
2.1	0.042	0.039
2.2	0.036	0.034
2.3	0.0310	0.0295
2.4	0.0275	0.0255
2.5	0.0240	0.0225
2.6	0.0215	0.0205
2.7	0.0195	0.0180
2.8	0.0175	0.0160
2.9	0.0160	0.0140
3.0	0.0135	0.0120
3.2	0.0088	0.0077
3.4	0.0072	0.0059
3.6	0.0064	0.0054
3.8	0.0061	0.0050
4.0	0.0059	0.0048
4.2	0.0061	0.0051
4.4	0.0056	0.0046
4.6	0.0045	0.0036

Table XXVI. (Cont'd.)

Energy (MeV)	Flux (neutrons/cm^2/MeV/min/W) Upper Limit	Lower Limit
4.8	0.0037	0.0028
5.0	0.0032	0.0025
5.2	0.00270	0.00215
5.4	0.00265	0.00195
5.6	0.00265	0.00200
5.8	0.0030	0.0023
6.0	0.0031	0.0024
6.2	0.00260	0.00195
6.4	0.0020	0.0014
6.6	0.0017	0.0011
6.8	0.00160	0.00105
7.0	0.00155	0.00102
7.2	0.00155	0.00100
7.4	0.00148	0.00098
7.6	0.00135	0.00089
7.8	0.00117	0.00076
8.0	0.00108	0.00066
8.2	0.00110	0.00068
8.4	0.00117	0.00076
8.6	0.00120	0.00081
8.8	0.00110	0.00070

Table XXVII. Unfolded NE-213 Spectrum 45 Deg Off the Centerline Behind 12 in. of Iron

Energy (MeV)	Flux (neutrons/cm^2/MeV/min/W) Upper Limit	Lower Limit
0.8	0.430	0.410
0.9	0.335	0.315
1.0	0.265	0.255
1.1	0.210	0.200
1.2	0.160	0.150
1.3	0.117	0.110
1.4	0.096	0.092
1.5	0.065	0.062
1.6	0.052	0.049
1.7	0.0425	0.040
1.8	0.036	0.034
1.9	0.0290	0.0275
2.0	0.024	0.022
2.1	0.0195	0.0180
2.2	0.0163	0.0148
2.3	0.0140	0.0123
2.4	0.012	0.0100
2.5	0.0102	0.0092
2.6	0.0087	0.0078
2.7	0.0075	0.0067
2.8	0.0067	0.0057
2.9	0.0056	0.0048
3.0	0.0048	0.0040
3.2	0.0041	0.0033
3.4	0.00355	0.00275
3.6	0.0031	0.0024
3.8	0.00280	0.00215
4.0	0.00245	0.00170
4.2	0.00175	0.00115
4.4	0.00140	0.00080

Table XXVII. (Cont'd.)

Energy (MeV)	Flux (neutrons/cm^2/MeV/min/W) Upper Limit	Lower Limit
4.6	0.00160	0.00102
4.8	0.00170	0.00110
5.0	0.00146	0.00090
5.2	0.00124	0.00066
5.4	0.00090	0.00051
5.6	0.00079	0.00034
5.8	0.00071	0.00026
6.0	0.00076	0.00033
6.2	0.00082	0.00039
6.4	0.00068	0.00029
6.6	0.00052	0.00012
6.8	0.00044	0.00006
7.0	0.00048	0.00012
7.2	0.00050	0.00017
7.4	0.00040	0.00011

The unfolded NE-213 spectral data behind 18 in. of stainless steel appear in Table XXVIII. Again, the limits of the spectrum at each energy are due to combined statistical and unfolding uncertainties.

Table XXVIII. Unfolded NE-213 Spectrum on the Centerline 47.7 in. Behind 18 in. of Stainless Steel

Energy (MeV)	Flux (neutrons/cm^2/MeV/min/W)	
	Upper Limit	Lower Limit
0.8	33.2	30.5
0.9	24.2	21.5
1.0	19.7	18.5
1.1	15.5	14.8
1.2	11.4	11.0
1.3	8.23	7.93
1.4	5.73	5.52
1.5	4.22	4.04
1.6	3.25	3.09
1.7	2.64	2.53
1.8	2.07	1.98
1.9	1.62	1.56
2.0	1.29	1.24
2.1	1.02	0.973
2.2	0.816	0.780
2.3	0.676	0.646
2.4	0.571	0.546
2.5	0.488	0.467
2.6	0.423	0.405
2.7	0.378	0.359
2.8	0.339	0.320
2.9	0.297	0.279
3.0	0.256	0.238
3.2	0.187	0.171
3.4	0.141	0.124

Table XXVIII. (Cont'd.)

Energy (MeV)	Flux (neutrons/cm^2/MeV/min/W) Upper Limit	Lower Limit
3.6	0.114	0.0977
3.8	0.113	0.0961
4.0	0.102	0.0851
4.2	0.0835	0.0686
4.4	0.0856	0.0713
4.6	0.0808	0.0678
4.8	0.0648	0.0523
5.0	0.0579	0.0455
5.2	0.0556	0.0430
5.4	0.0551	0.0433
5.6	0.0471	0.0358
5.8	0.0428	0.0317
6.0	0.0424	0.0317
6.2	0.0388	0.0284
6.4	0.0350	0.0243
6.6	0.0334	0.0225
6.8	0.0371	0.0266
7.0	0.0391	0.0291
7.2	0.0298	0.0199
7.4	0.0170	0.00719
7.6	0.0182	0.00866
7.8	0.0284	0.0193
8.0	0.0309	0.0228
8.2	0.0232	0.0154
8.4	0.0170	0.00915
8.6	0.0176	0.0101
8.8	0.0198	0.0125
9.0	0.0194	0.0125
9.2	0.0184	0.0115
9.4	0.0177	0.0109
9.6	0.0178	0.0113
9.8	0.0188	0.0123
10.0	0.0182	0.0117

Analysis

In the analysis of the experiment Monte Carlo calculations of the transport of neutrons above thermal energies were performed using the multigroup code MORSE.[9] For the calculations of the transmitted fluxes through the iron slabs, three sets of basic iron cross-section data were used, designated MAT 1101,[10] MAT 1124,[11] and MAT 4180-Mod. 1.[12] Major comparisons of the neutron cross sections for these three evaluations are summarized in Table XXIX.

Table XXIX. Major Comparisons of the Neutron Cross Sections for the Three Iron Evaluations

	MAT 1101	MAT 1124	MAT 4180-Mod. 1
Total Cross Sections in the range 100 eV <E< 20 keV	In general, higher above 5 keV, lower below 5 keV than 1124 or 4180-Mod. 1	Identical	Identical
Total Cross Section Minimum near 24 keV	650 mb	290 mb	420 mb
Total Cross Sections in the range 80 keV <E< 800 keV	Identical	Identical	In general, deeper and/or broader minima than 1101 or 1124
Total Cross Sections in the range 800 keV <E< 15 MeV	Identical	Identical	Identical
Partial Inelastic Scattering Cross Sections	Nothing above 5 MeV	Values above 5 MeV including both levels and continuum.	First excited level excitation function different from either 1101 or 1124.
Elastic Scattering Angular Distributions in the range 400 keV <E< 15 MeV		Different above 4.6 MeV from 1101	Same as 1124 above 4.6 MeV, different from either 1101 or 1124 in range 0.4 MeV <E< 1.4 MeV.

Note that the ENDF/B-III version for iron, MAT 1180, was not one of the sets used. It differs from the MAT 1124 set only in that the total cross section minimum in the vicinity of 24 keV was changed from ∿280 mb to 420 mb. Thus, all spectral comparisons for the NE-213 and Benjamin counter using the 1124 set would be identical to those using the 1180 set. Only the calculated Bonner ball counting rates would be expected to be somewhat different using these two sets, due to the difference in the transmitted fluxes from the vicinity of 24 keV and below.

The basic cross section data used for the carbon and manganese components in the iron transmission calculations were ENDF/B evaluations which were essentially the same as the ENDF/B-III sets designated by MAT numbers 1165 and 1019 respectively. The point data for carbon steel were processed with SUPERTOG[13] into a set of multigroup cross sections weighted $1/E\sigma_{T_{Fe}}$ having a slightly different group structure depending on the particular iron evaluation used. For MAT 1101 data, a 215-group structure was used; for MAT 1124 data, a 218-group structure was used; and for MAT 4180-Mod. 1 data, a 220-group structure was used. All the group structures were designed to conform to the structure in the iron total cross section, with particular emphasis on the total cross-section minima. The 220-group structure was presented in Table III; the 218- and 215-group structures differ in slight detail in the energy region 19 keV $\leq E \leq$ 493 keV. For all three group structures, the first 132 groups (0.493 MeV $\leq E \leq$ 10 MeV) and the last 18 groups (thermal $\leq E \leq$ 19 keV) are identical. A measure of the importance of selecting the multigroup structure is the comparison of a 100-group (GAM-II) calculation with a 220-group calculation of the neutrons leaking a 1-meter radius sphere from a point fission source located at the center. (See Appendix.)

Both cross-section sets were based on the same 4180-Mod. 1 data with $1/E\sigma_T$ group weighting. The differences are alarming.

The multigroup sets used expansion through P_3 for the elastic scattering angular distributions and through P_0 for the nonelastic scattering angular distributions. In addition to the multigroup sets, total macroscopic cross-section data at over 6000 energy points in the region 15 keV to 10 MeV were incorporated into MORSE. The "point" data were used to calculate the uncollided flux analytically, as well as to sample more accurately the location of the next collision point in the random walk procedure and the next flight estimator in the statistical estimation technique.

Calculations through 12 in. of stainless steel were carried out using multigroup sets based only on the MAT 1124 and a preliminary version of the MAT 4180-Mod. 1 evaluations. The latter set was very similar, although not identical, to the final version used in the iron calculations and differed from the final version in that it incorporated preliminary rather than final results of the measurements of Harvey[14] of the total cross-section minima in the region 80 to 493 keV; also, it did not incorporate all of the cross-section changes in the MeV region made in the final version. Calculations through 18 in. of stainless steel used a multigroup set based on the preliminary version of MAT 4180-Mod. 1 only. The basic cross-section data used for the chromium, nickel, and manganese components were ENDF/B evaluations which were essentially the same as the ENDF/B-III sets designated by MAT numbers 1121, 1123, and 1019, respectively. The same 218-group structure was used with both iron evaluations. The total macroscopic cross-section data at over 6000 energy points for the stainless steel were based on the same iron data sets used to generate the multigroup sets for all the

calculations behind 12 in. of stainless steel, and on the final 4180-Mod. 1 set for all the calculations behind 18 in. of stainless steel.

Since the experiment can be adequately represented geometrically as two dimensional (the 5-ft-square slabs can be treated as cylinders of 5.64-ft-diam with negligible error since differences in the two transverse leakages are small), the calculations employed cylindrical symmetry in describing the reactor collimator and the iron collar and water shield surrounding it. Effects due to multiple reflection between the slab samples and the reactor collimator, including both the iron collar and water shield surrounding the collimator, were explicitly and separately calculated and were added to the results obtained with a vacuum boundary at the front and back of the slabs. The approximate enhancement of the slab-scattered transmitted fluxes due to this collimator effect is shown in Table XXX.

Table XXX. Calculated Enhancement of the Transmitted Slab-Scattered Flux Above Thermal Energy Arising from Reflection off the Collimator

	ϕ Total Including Collimator/ϕ Total Not Including Collimator
Behind 1-1/2 in. of Iron	1.11
Behind 12 in. of Iron	1.21
Behind 24 in. of Iron	1.21
Behind 36 in. of Iron	1.10
Behind 12 in. of Stainless Steel	1.17
Behind 18 in. of Stainless Steel	1.08

Uncollided air attenuation was not considered in the calculations of the slab transmitted fluxes at the detector locations behind the slabs, but this can lead to overestimates of the calculated fluxes only by approximately 5%.

The calculations employed little biasing since the most important effect of the many windows in iron, which control the transmission, is easily calculated provided the cross-section structure is represented in

adequate detail. For the thicker slabs, the biasing used consisted of incorporating a value of the path length stretching parameter (XNU) of 0.5 for all energies above 10 keV and 0.75 for all energies below 10 keV for all but the last 6 inches of the slab, where it was 0.0. Non-escape biasing was applied in the last 6 inches of the slab. Weight standards for playing Russian roulette were conservatively low, so that very few neutrons were killed.

Only slab-scattered fluxes were calculated by Monte Carlo. Statistics on the calculated fluxes were, in general, adequate (20% or better) for each energy group except in the energy range below ~1 keV behind at least a foot of iron, where they were poor. Since the contribution of these poorly calculated low-energy fluxes to the Bonner ball counting rates is only at most 15% for the 3-in. ball and negligible for the others, little effort was expended in attempting to improve these calculations. Statistics on the calculated Bonner ball counting rates arising from slab-scattering even behind 36 in. of iron averaged 15% for the 3-in. ball and 5% for the 6-in. and 10-in. balls.

Uncollided fluxes incident on the centerline detectors were analytically calculated from the previously measured geometric attenuation of the source beam and incorporating exponential attenuation based on the point total cross-section data. For the iron and 12 in. of stainless steel calculations which employed the collimator shown in Fig. 1, the following equation was used:

$$\phi_{unc}(Z,E_g) = \phi_0(E_g) \times (68/68+Z)^2 \int_{E_{g_\ell}}^{E_{g_u}} \exp\left(-\Sigma_T[Z]T\right) dE/(E_{g_u}-E_{g_\ell}) , \qquad (1)$$

where the $\Sigma_T(E)$ are "point" values, the $\phi_0(E_g)$ were taken directly from Table III for the 220-group structure and from similar tables for the

215 and 218 group structures, E_{g_u} and E_{g_ℓ} are the upper and lower limits of the group E_g, T is the thickness of the slab in cm, and Z is the distance from the detector to the open end of the collimator in inches. For the calculations through 18 in. of stainless steel which employed the collimator shown in Fig. 3, a similar equation was used:

$$\phi_{unc}(Z,E_g) = \phi_0(E_g) \times (59.5/59.5+Z)^2 \int_{E_{g\ell}}^{E_{g_u}} \exp\left(-\textstyle\sum_T [E]T\right)dE/(E_{g_u} - E_{g_\ell}) , \quad (2)$$

where the $\phi_0(E_g)$ were taken from an appropriately regrouped form of the entries in Table VI.

Comparison of the Calculated and Measured Low Energy Spectra Behind 1/2-in. Iron

Calculations of the low-energy spectra behind 1/2-in. of iron were made using the MAT 1101 set for iron. No multiple reflection between the collimator and the slab was considered, so that the off-centerline comparisons are probably undercalculated by approximately 10%. Comparisons of the calculated thermal fluxes (E<0.4 eV) with the measured values are shown in Table XXXI.

Table XXXI. Comparison of Measured and Calculated Thermal Fluxes Behind 1/2 in. of Iron in Neutrons/cm^2/min/W

	On Centerline	At 15 Degrees	At 45 Degrees
Measured	212	1.53	0.862
Calculated	205	0.854	0.675
Calculated/Measured	0.97	0.56	0.78

The comparisons of the calculated and measured fluxes from 0.4 eV to 4 keV are shown in Fig. 4 for the three detector locations. For both the

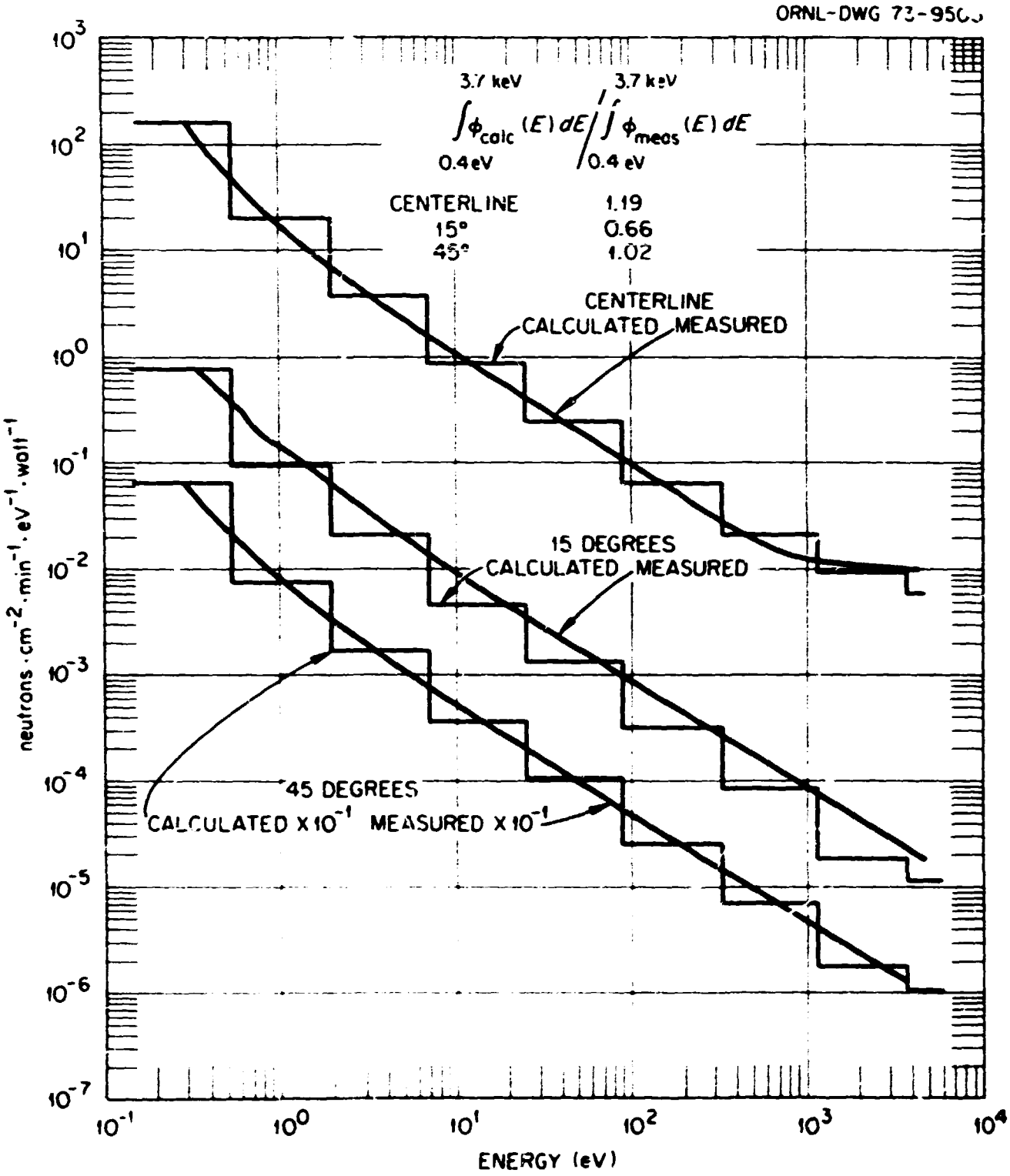

Fig. 4. Comparison of Measured and Calculated Low Energy Spectra Behind 1/2 in. of Iron.

thermal and non-thermal neutrons, the agreement on the centerline, where the uncollided flux is better than 99% of the total flux, and at 45 degrees lies within the uncertainty of the source spectrum (estimated to be ±20%). There appears to be a serious disagreement at 15 degrees, where the calculations underpredict the measurements. It is believed the disagreement at 15 degrees is most probably caused by the presence in the measurement of a small uncollided component which was not assumed in the calculation. This uncollided tail at 15 degrees need only be of the order of 1/2% of the centerline uncollided component to be of the same intensity as the scattered flux at 15 degrees.

Comparison of the Calculated and Measured Low Energy Spectra Behind 1-1/2 in. Iron

Comparisons of the low-energy spectra behind 1-1/2 in. of iron were also made using the MAT 1101 set for iron. Effects of multiple reflection between the collimator and the slab were considered, and amounted to increases in the slab-scattered fluxes below ~1 keV of the order of 25%. Comparisons of the calculated thermal fluxes (E<0.4 eV) with the measured values are shown in Table XXXII.

Table XXXII. Comparison of Measured and Calculated Thermal Fluxes Behind 1-1/2 in. of Iron in Neutrons/cm^2/min/W

	On Centerline	At 15 Degrees	At 45 Degrees
Measured	14.2	0.453	0.283
Calculated	12.3	0.425	0.261
Calculated/Measured	0.87	0.94	0.92

The comparisons of the calculated and measured fluxes from 0.4 eV to 4 keV are shown in Fig. 5 for the three detector locations. For both the thermal and non-thermal neutrons, the agreement at 15 and 45 degrees is adequate. On the centerline, the agreement is adequate for the thermal neutrons and poor for the non-thermal neutrons, where in the latter case the calculations overpredict the measurement by a factor of two. The uncollided fluxes on the centerline comprise about 96% of the total flux. No reason can be given for this disagreement, other than to state that the unfolded spectrum appears questionable in the energy range above 2 eV, in particular the dip that occurs at 5 eV and the low flux levels between 1 keV and 4 keV. Because the neutron cross sections for iron in this low-energy region are reasonably well known, all but perhaps the 15 degree comparison behind 1/2 in. of iron illustrate the general accuracy of the results to be expected from the use of unfolding the ^{10}B spectrometer counting rates, since the low-energy source terms used in the calculations were also derived from counting rates using the ^{10}B spectrometer.

Comparison of the Calculated and Measured Bonner Ball Counting Rates In the Free Field

The calculated Bonner ball counting rates, in general, involved folding the calculated fluxes at the center of detection of each Bonner ball with the corresponding response function of the Bonner ball. The response functions appear in Figs. 6-8, and are tabulated in Refs. 6 and 14. As a check on both these response functions and the source terms appearing in Table III for the 4-1/4-in. collimator, calculations of the fluxes at the center of detection of the three Bonner balls were made using the following:

$$\phi(E_g, Z) = \phi_0(E_2) \times (68/68+Z)^2 \qquad (3)$$

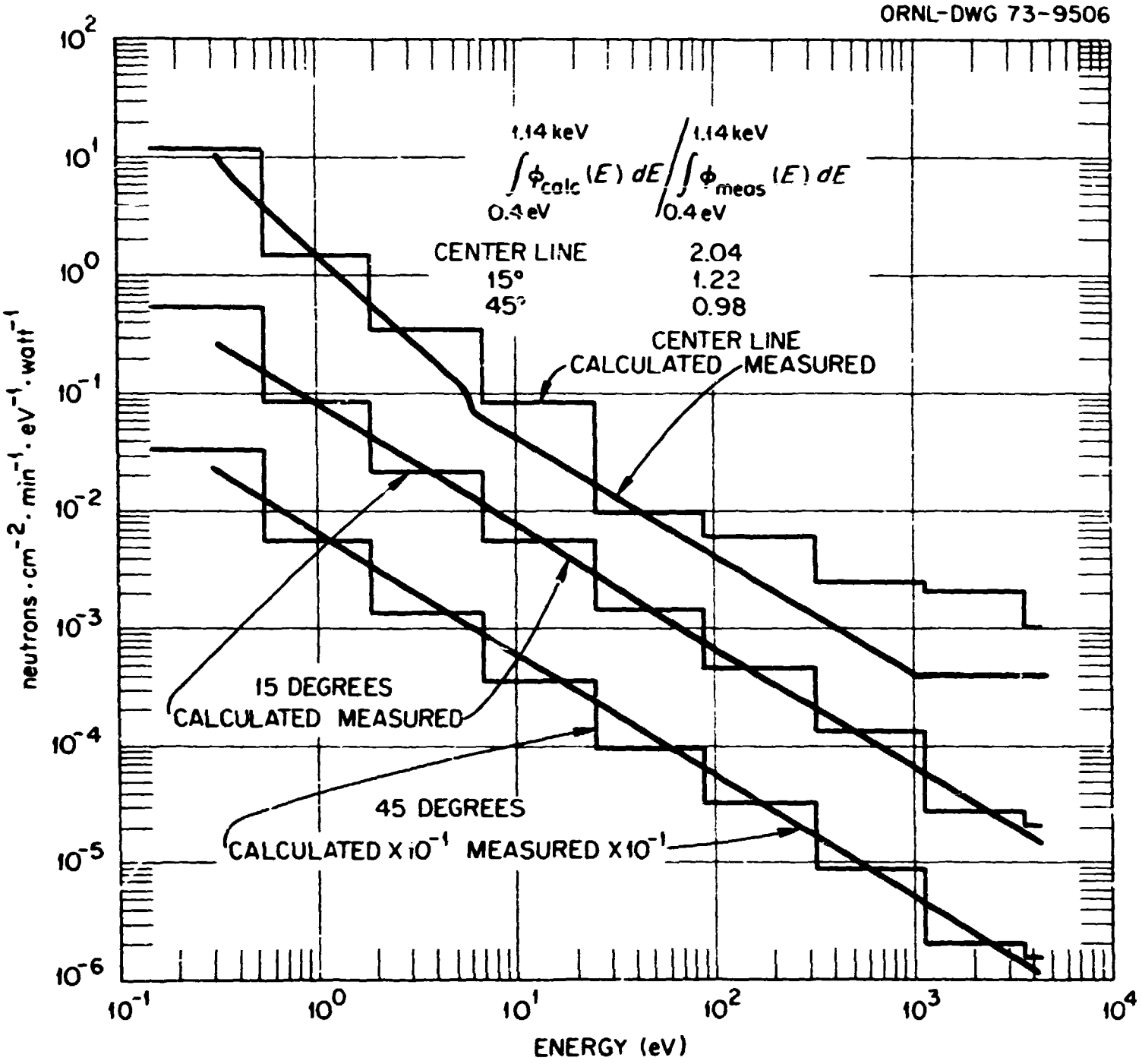

Fig. 5. Comparison of Measured and Calculated Low Energy Spectra Behind 1-1/2 in. of Iron.

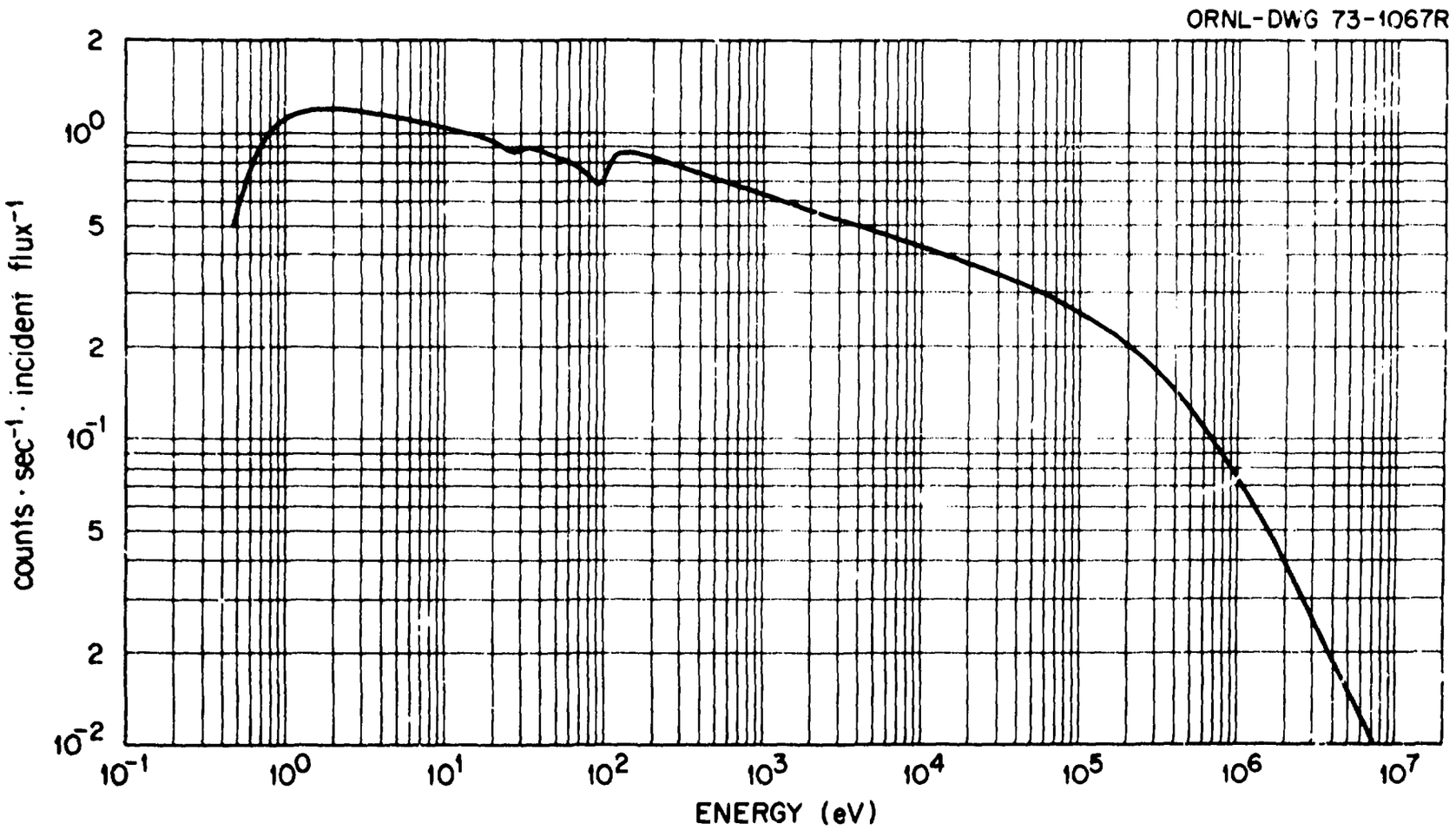

Fig. 6. Three-Inch Bonner Ball Response Function.

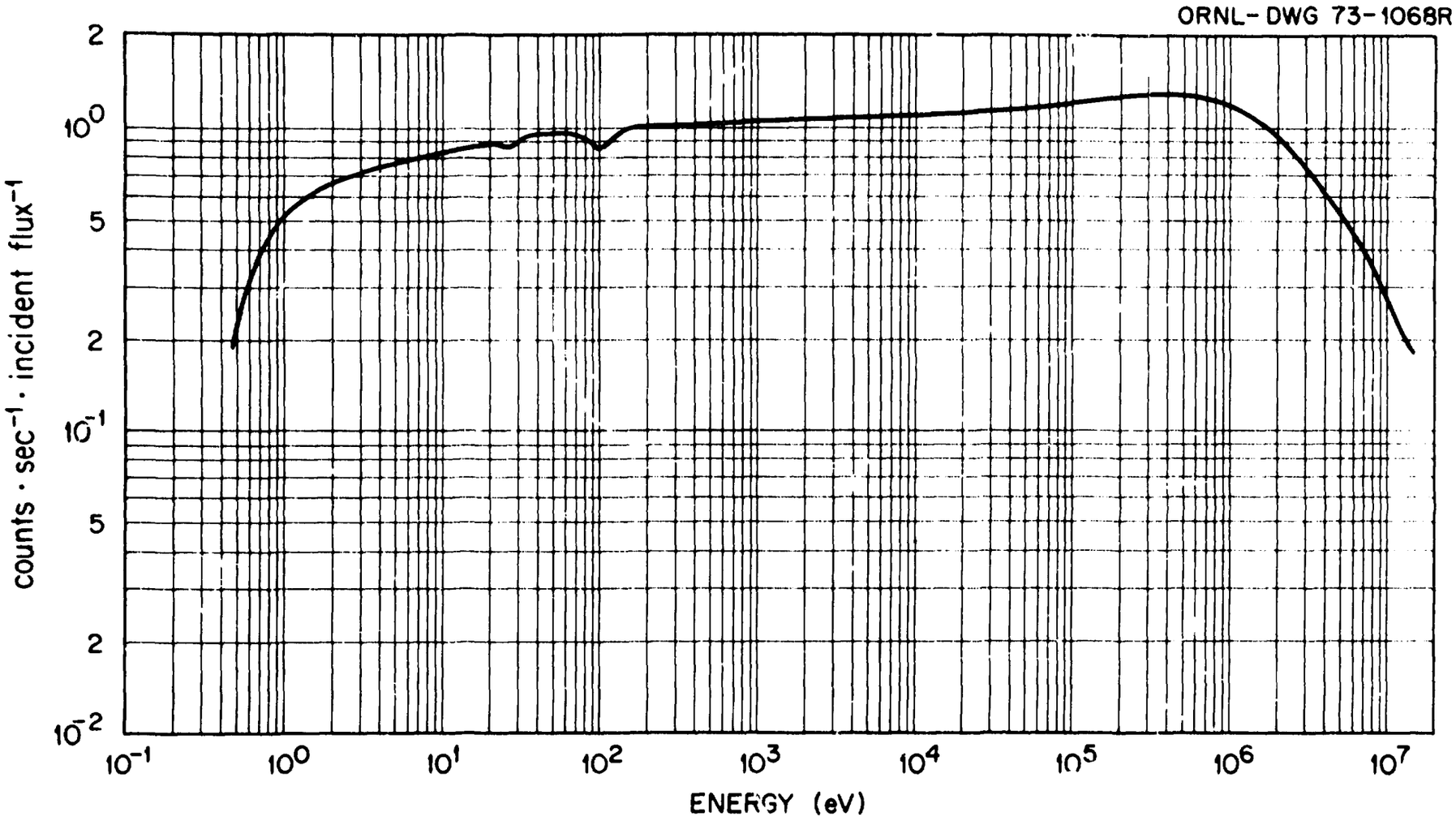

Fig. 7. Six-Inch Bonner Ball Response Function.

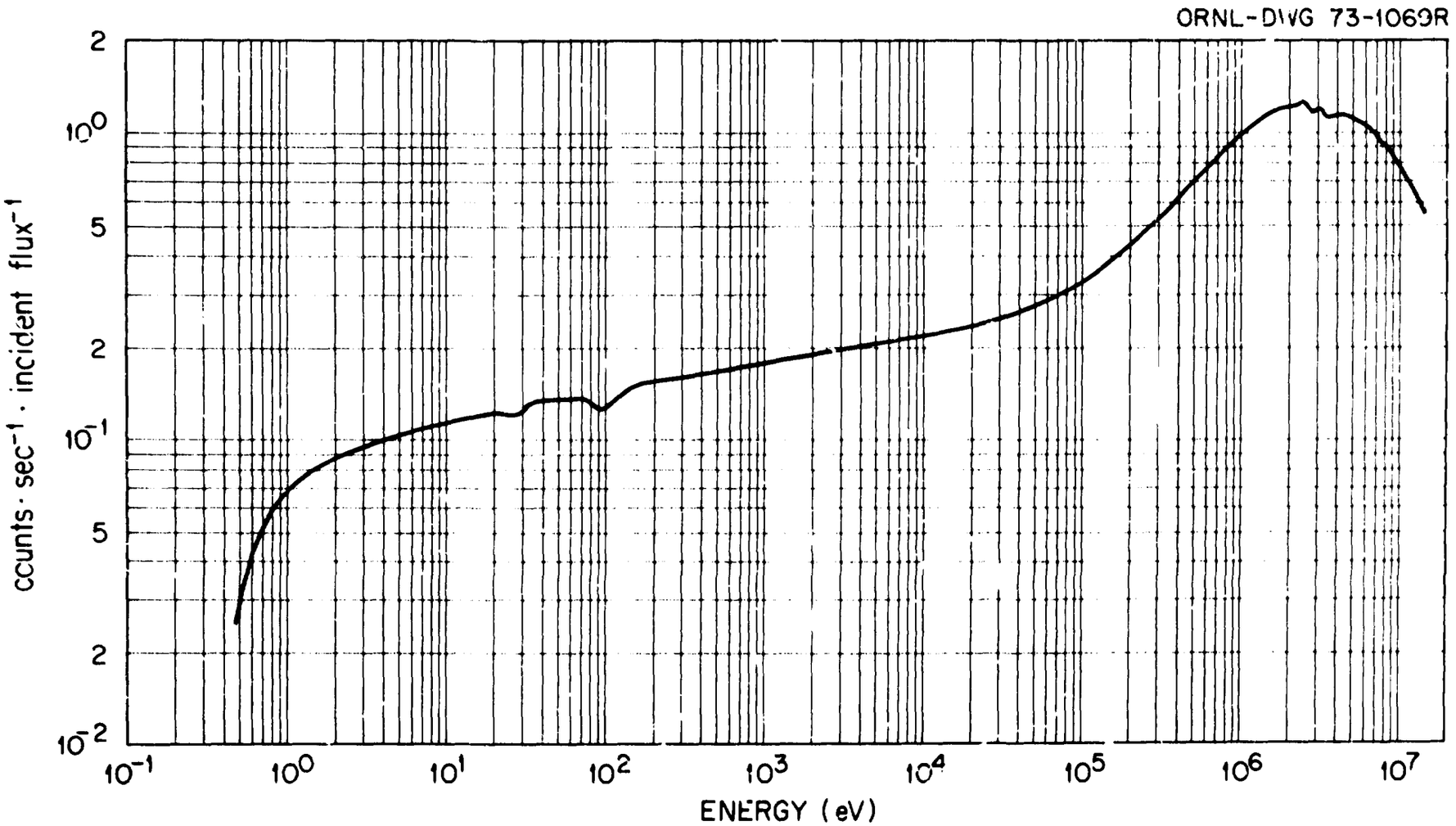

Fig. 8. Ten-Inch Bonner Ball Response Function.

where Z represents the distance in inches from the outside edge of the iron collar in Fig. 1 to the center of detection of each ball, and the $\phi_0(E_g)$ represent the entries in Table III. Since the measured counting rates were made at a constant distance of 153 in. between the edge of the iron collar and the geometric center of each ball, Z assumes the values 152.1 in., 151.2 in., and 150 in. for the 3-in., 6-in., and 10-in. balls, respectively (see Table II). The corresponding counting rates were calculated from:

$$\text{Counting Rate}_{BB}(Z) = \int_{0.4\ eV}^{10\ MeV} \phi\ (E_g, Z) R_{BB}(E_g) dE_g\ , \qquad (4)$$

where the $R_{BB}(E_g)$ are the response functions for each of the three Bonner balls. A comparison of the calculated and measured Bonner ball counting rates is shown in Table XXXIII.

Table XXXIII. Comparison of Calculated and Measured Free Field Bonner Ball Counting Rates 153 in. from the Collimator in Counts/min/W

Bonner Ball	3-in.	6-in.	10-in.
Measured	469	1980	1699
Calculated	508	2120	1857
Calc/Measured	1.08	1.07	1.09

The comparisons are within 10%, which is within the accuracy to which the absolute free field and response functions are known. Similar comparisons using the 15-1/4-in. collimator of Fig. 3 and the source terms in Table VI were made and appear in Reference 15. These latter comparisons are also within 10%.

Bonner Ball Comparisons Behind 1-1/2 in. of Iron

Calculations of the Bonner ball counting rates behind 1-1/2 in. of iron were made using each of the three iron cross-section sets designated MAT 1101, MAT 1124, and MAT 4180-Mod. 1. The effects of collimator scattering are included in the final results, which are compared with the measurements in Table XXXIV.

Table XXXIV. Comparison of Measured and Calculated Bonner Ball Counting Rates Behind 1-1/2 in. of Iron in Counts/min/W

Bonner Ball	3-in.			6-in.			10-in.		
	CL	15°	45°	CL	15°	45°	CL	15°	45°
Measured	57.8	1.02	0.680	607	5.22	2.82	587	4.74	1.99
Calculated (1101)	66.2	0.990	0.676	648	4.65	2.94	638	4.23	2.26
Calculated (1124)	64.8	1.02	0.680	649	4.75	2.95	649	4.38	2.30
Calculated (4180-Mod. 1)	64.8	1.02	0.680	636	4.61	2.86	618	4.18	2.19
Calculated (1101)/Meas.	1.14	0.97	0.99	1.07	0.89	1.04	1.09	0.89	1.14
Calculated (1124)/Meas.	1.12	1.00	1.00	1.07	0.91	1.05	1.11	0.92	1.16
Calculated (4180-Mod. 1)/Meas.	1.12	1.00	1.00	1.05	0.88	1.01	1.05	0.88	1.10

Since the slab is so thin, the net effects of different cross-section sets on the counting rates behind the slab are very small, and they are partially obscured by the statistics of each calculation which is of the

order of 1%. The comparisons do indicate the correctness of the Monte Carlo procedure and serve as a check on the input data used in the calculations. The slight discrepancy at 15 degrees for the 6- and 10-in. Bonner balls is most probably due to the presence of a small uncollided component in the measurement, since the calculated counting rate at 15 degrees is less than 1% of the centerline counting rate, over 98% of which is due to uncollided neutrons. Thus, the uncollided contribution at 15 degrees need only be of the order of 0.2% of the centerline contribution to account for the ~10% disagreement at 15 degrees. Since this small fraction is far less than the background measurement at 15 degrees in the free field and could not be measured, it could not be incorporated into the calculations.

NE-213 Comparisons Behind 4 in. of Iron

The off-centerline calculations of the neutron spectra above 0.82 MeV behind 4 in. of iron were made for each of the three iron cross-section sets. Comparisons of the calculations integrated over the energy range 0.82-9 MeV with measured values are shown in Table XXXV.

Table XXXV. Comparison of NE-213 Integrated Spectra Above 0.82 MeV with Calculated Values Behind 4 in. of Iron in Neutrons/cm^2/min/W

	15 Degrees		45 Degrees	
	Results	Calc/Meas	Results	Calc/Meas
Measured	1.74		0.846	
Calculated (1101)	1.76	1.01	0.918	1.08
Calculated (1124)	1.86	1.09	0.952	1.15
Calculated (4180-Mod. 1)	1.87	1.09	1.02	1.23

Since the total cross sections in this energy range are identical for the three sets, the differences between the calculations arise as a result of differences in the angular distributions of elastic scattering and differences in the partial inelastic scattering cross sections. All three sets lead to about the same integrals, with the oldest set (MAT-1101) agreeing slightly better with the measurements. It should be emphasized, however, that the processing code treats all inelastic scattering as isotropic, so that any anisotropies in inelastic scattering present in the evaluated data set are absent in the multigroup representation. The importance of the P_0 truncation of the inelastic scattering angular distributions in affecting the off-centerline calculations in this experiment is unknown, but if this approximation could be avoided, it may well change the calculations enough to alter any conclusion regarding which of the three sets is superior. Further, all the angular distributions arising from elastic scattering are processed only through P_3, and this approximation can also lead to disagreement for those energy regions where the scattering is highly anisotropic. Thus, further calculations of the off-centerline fluxes using all the angular distribution data in a "point" Monte Carlo code for each evaluated set are necessary before definite conclusions can be drawn about the adequacy of the angular distribution data in the energy region above 0.8 MeV. All that can be said now is that use of a group processing code with P_3 and P_0 truncations of the angular distributions arising from elastic and inelastic scattering, respectively, plus point total cross sections yields calculated fluxes that agree within ~20% of experiment for the off-centerline detectors, and that the MAT 4180-Mod. 1 set yields adequate agreement at 15 degrees and is a little high at 45 degrees.

The spectra calculated using MAT 4180-Mod. 1 were smoothed with the resolution function of the NE-213 spectrometer[14] and are compared with the measurements in Figs. 9 and 10. In general, undulations in the smoothed calculated spectra above 3 MeV are due to the coarse group structure used in the calculations, i.e., 3 to 4 MeV, 4 to 5 MeV, 5 to 6 MeV, 6 to 8 MeV, and 8 to 10 MeV. Since the source spectrum (see Fig. 2) decreases smoothly with increasing energy above 3 MeV, the effect of the coarse group structure, even after smoothing, is, for example, to underestimate the flux in the region 3 to 3.5 MeV, overestimate the flux in the region 3.5 to 4 MeV, underestimate the flux in the region 6 to 7 MeV, overestimate the flux in the region 7 to 8 MeV, etc. These undulations are particularly evident in Figs. 9 and 10. In Fig. 9, slight overpredictions are seen to occur in the vicinity of 0.8 MeV, 2 MeV, and 3.5 MeV, but the general agreement is adequate. In Fig. 10, the calculations overpredict the measurements everywhere above ~1.5 MeV, with the disagreement above ~3 MeV being well outside the statistics of the calculations, which appear in the figures as ± one standard deviation.

NE-213 Comparison Behind 6 in. of Iron

The calculations for a detector on the centerline behind 6 in. of iron for all three data sets are nearly identical (within 1%) since the calculated uncollided component comprises approximately 95% of the total flux and the total cross section in this energy range is the same for each set. The smoothed calculated spectrum is compared with the measurement in Fig. 11. The agreement behind 6 inches of iron is in general very good, and only in the regions centered around 1.5 MeV and 2.5 MeV does there appear to be any significant discrepancy. These disagreements suggest that the average total cross section in these regions is too high by about 5% in the data sets used.

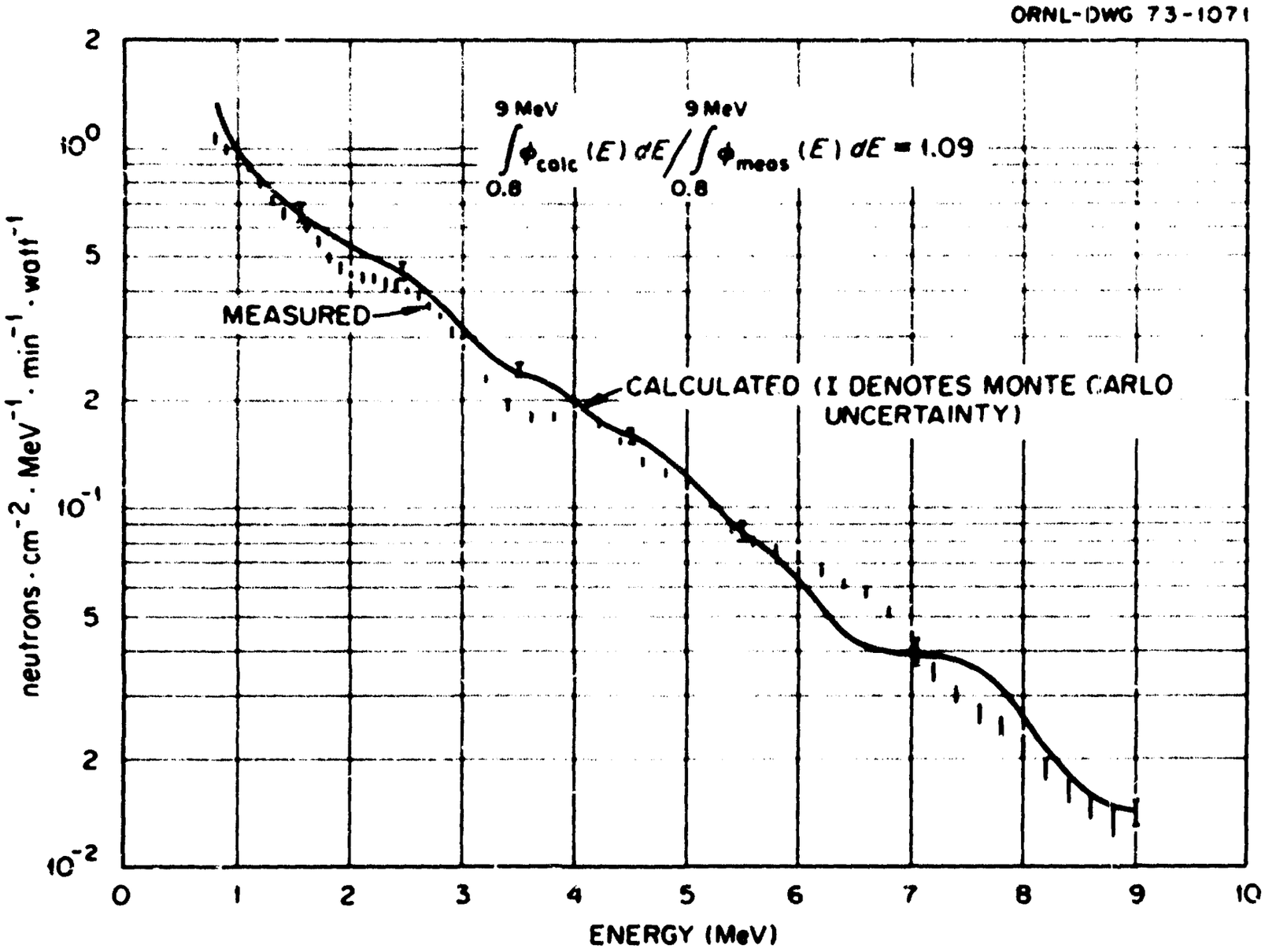

Fig. 9. Comparison of Calculated and Measured Spectra Above C.8 MeV at 15 Degrees Behind 4 in. of Iron. Calculations used the MAT 4180-Mod. 1 set.

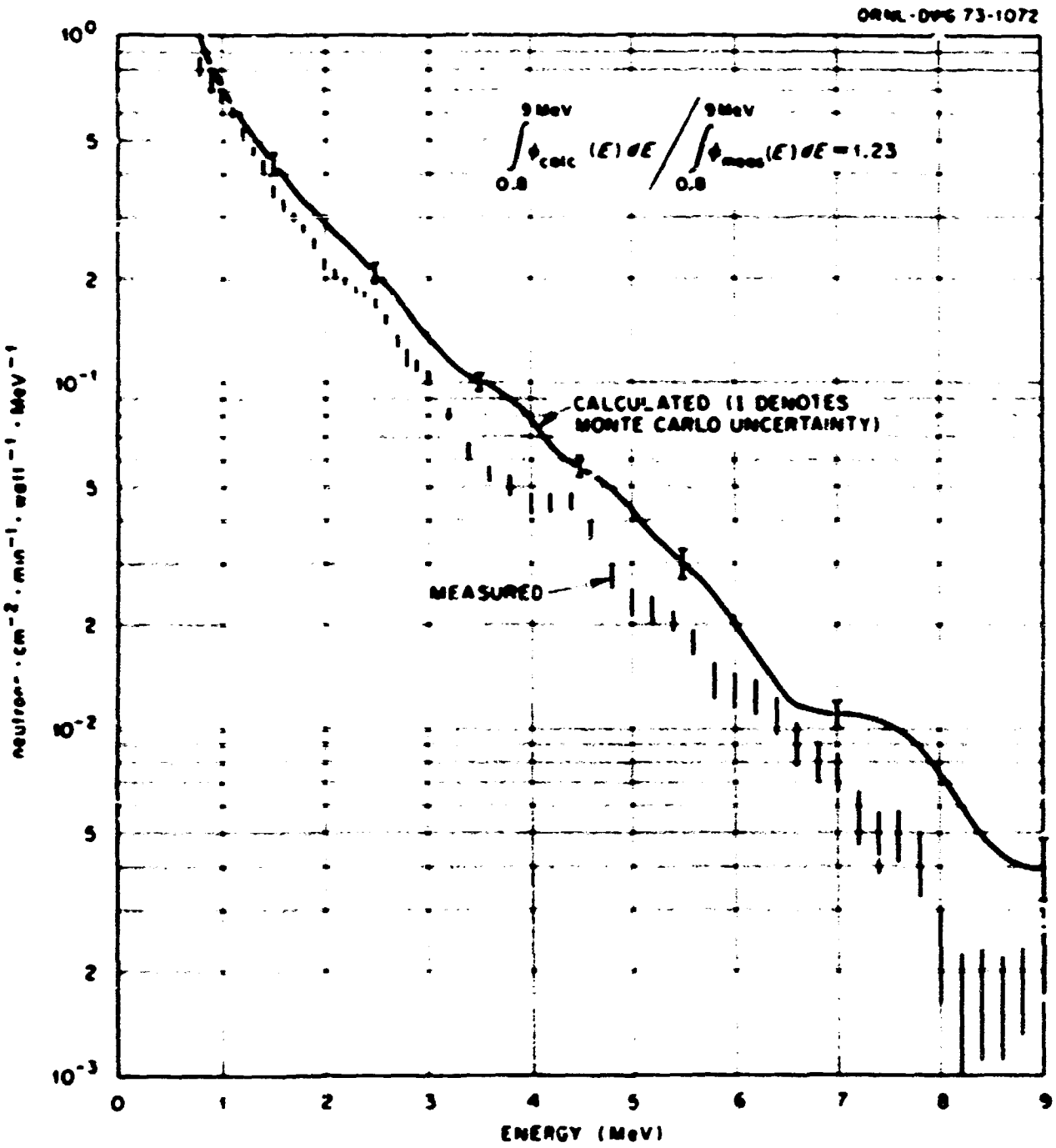

Fig. 10. Comparison of Calculated and Measured Spectra Above 0.8 MeV at 45 Degrees Behind 4 in. of Iron. Calculations used the MAT 4180-Mod. 1 set.

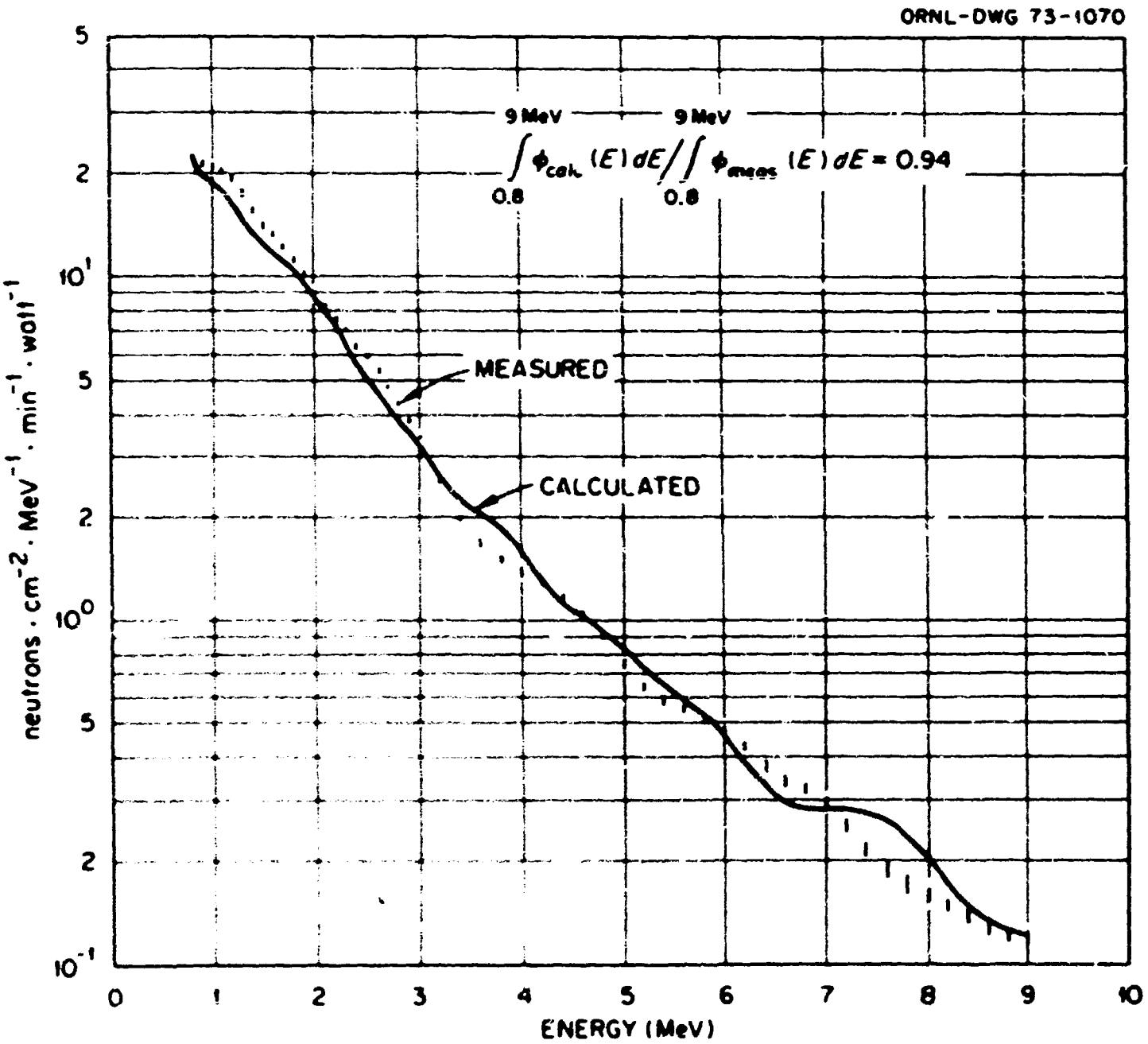

Fig. 11. Comparison of Calculated and Measured Neutron Spectra Above 0.8 MeV on the Centerline Behind 6 in. of Iron. Calculations using all three data sets for iron give essentially the same spectrum.

NE-213 Comparisons Behind 12 in. of Iron

The calculations for a detector on the centerline behind 12 in. of iron for all three data sets again are nearly identical since the calculated uncollided component comprises approximately 88% of the total flux. The smoothed calculated spectrum is compared with the measurement in Fig. 12. The agreement behind 12 inches of iron is very poor, and the comparison indicates that the average total cross section in the region ~1 to 3 MeV is too high by approximately 8 percent in the data sets used. This measurement tests the total cross section much more sensitively than the centerline measurement behind 6 inches of iron, and hence determines any errors in the total cross section far more accurately. This significant disagreement between the measured and calculated spectra is consistent with a similar disagreement between the measured and calculated uncollided flux behind 12 in. of iron that was found in an earlier experiment.[16] The point total cross-section data in the region 0.8 to 10 MeV used in MAT 1101, MAT 1124, MAT 1180, MAT 4180, and MAT 4180-1 are identical and based on the measurements of Cerbone.[17] These measurements were made with considerably better resolution than those performed earlier at Karlsruhe,[18] and showed deeper minima in the interference regions of the total cross section. It is conjectured that a cross-section measurement performed either with better resolution or through a thicker sample than that used by Cerbone might indicate the presence of even deeper minima, and might well produce results more in agreement with the measurement in Fig. 12.[19] The calculated spectra in Fig. 12 are very sensitive to these minima since the uncollided weighting factor for each point total cross section is proportional to $\exp(-2.60\sigma_t)$, where σ_t is in barns. Thus, the average cross section in the range E_1 to

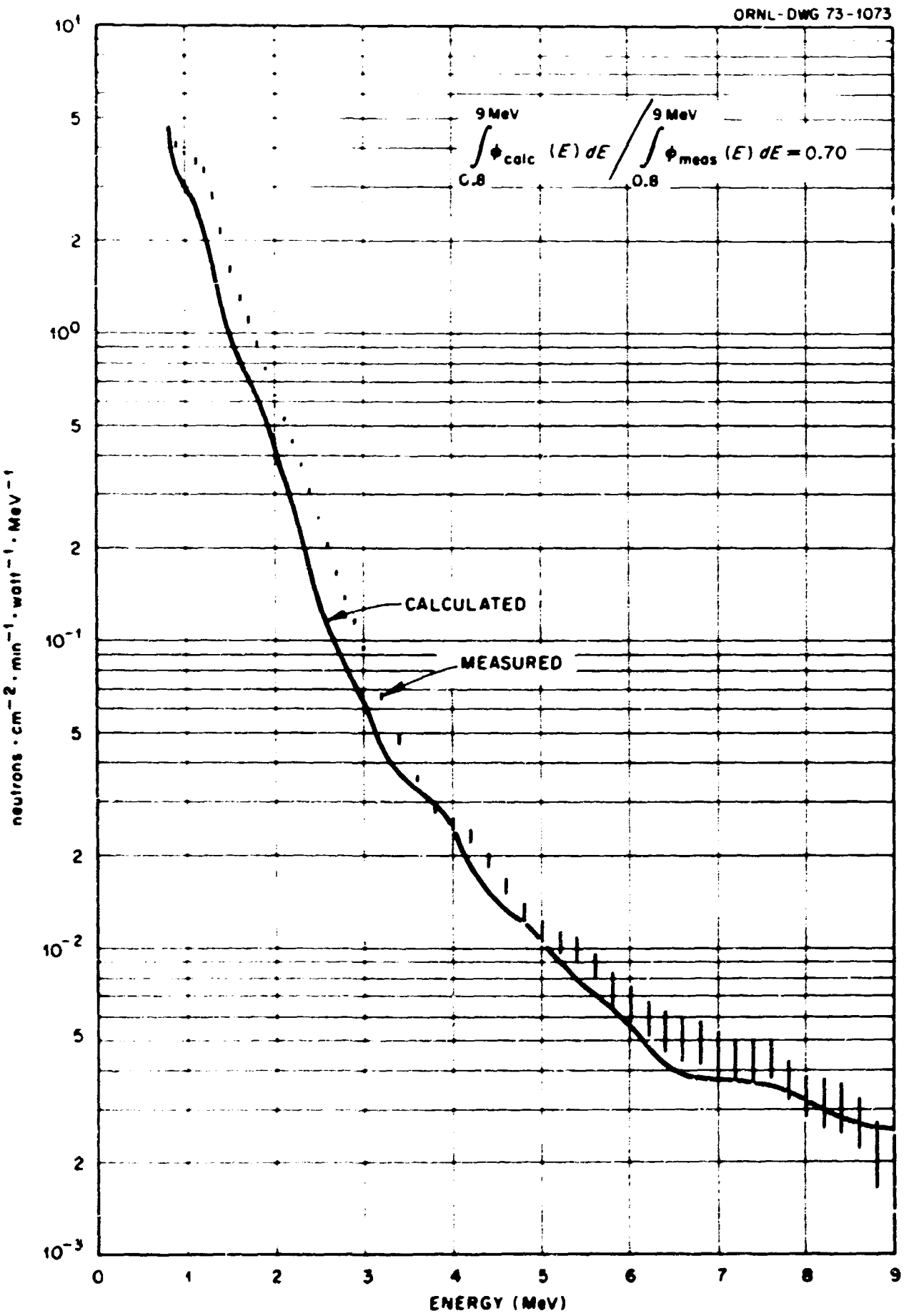

Fig. 12. Comparison of Calculated and Measured Spectra Above 0.8 MeV on the Centerline Behind 12 in. of Iron. Calculations using all three data sets for iron give essentially the same spectrum.

E_2 is:

$$\bar{\sigma}_t = \int_{E_1}^{E_2} S(E)\ \sigma_t(E)\ \exp(-2.60\sigma_t)\ dE \Big/ \int_{E_1}^{E_2} S(E)\ \exp\ (-2.60\sigma_t)\ dE, \quad (5)$$

where S(E) is the source spectrum appearing in Table III. It is the quantity $\bar{\sigma}_t$ that is about 8% too high in the region ~1 to 3 MeV.

Calculations for the off-centerline detectors behind 12 in. of iron were made with each of the three data sets for iron. A comparison of the calculated integrated spectra over the energy range 0.82 to ~8 MeV with measured values is shown in Table XXXVI.

Table XXXVI. Comparison of NE-213 Integrated Spectra Above 0.82 MeV With Calculated Values Off the Centerline Behind 12 in. of Iron in Neutrons/cm^2/min/W

	15 Degrees		45 Degrees	
	Results	Calc/Meas	Results	Calc/Meas
Measured	0.265		0.157	
Calculated (1101)	0.196	0.74	0.106	0.67
Calculated (1124)	0.192	0.73	0.100	0.64
Calculated (4180-Mod. 1)	0.247	0.93	0.128	0.81

From an inspection of Table XXXVI, it is to be observed that the MAT 4180-Mod. 1 data set is significantly better in predicting the off-centerline fluxes behind 12 in. of iron. The range of scattering angles that the neutrons undergo in reaching off-centerline detectors is far greater in penetrating 12 in. of iron than 4 in. of iron, since many of the neutrons leaking the 12 in. slab are multiply-scattered. Hence, for

example, the ~20% overprediction of scattering in the vicinity of 45 degrees observed behind 4 in. of iron and the ~20% underprediction observed at the same angle behind 12 in. of iron are not necessarily incompatible.

The smoothed calculated spectra using the MAT 4180-Mod. 1 set are compared with the measurements in Figs. 13 and 14 for the off-centerline detectors. The only disagreement outside the statistics of the calculation occurs in the energy region ~1 MeV to 1.5 MeV for the 45 degree case.

Benjamin Counter Comparisons Behind 12 in. of Iron

Calculations of the spectra in the energy region ~60 keV to ~1.5 MeV were made for the Benjamin counter locations behind 12 in. of iron using the MAT 1124, MAT 4180-Mod. 1, and the preliminary version of the MAT 4180-Mod. 1 data sets for iron. A comparison of the integrated results over the energy range 90 keV to 1.3 MeV between the calculations and the measurements is shown in Table XXXVII.

Table XXXVII. Comparison of Integrated Benjamin Counter Spectra With Calculated Values Behind 12 in. of Iron in Neutrons/cm^2/min/W

	On the Centerline		Off the Centerline	
	Results	Calc/Meas	Results	Calc/Meas
Measured	174		74.5	
Calculated (4180-Mod. 1, prel.)	197	1.13	83.6	1.12
Calculated (4180-Mod. 1)	179	1.03	80.0	1.07
Calculated (1124)	170	0.98	83.5	1.12

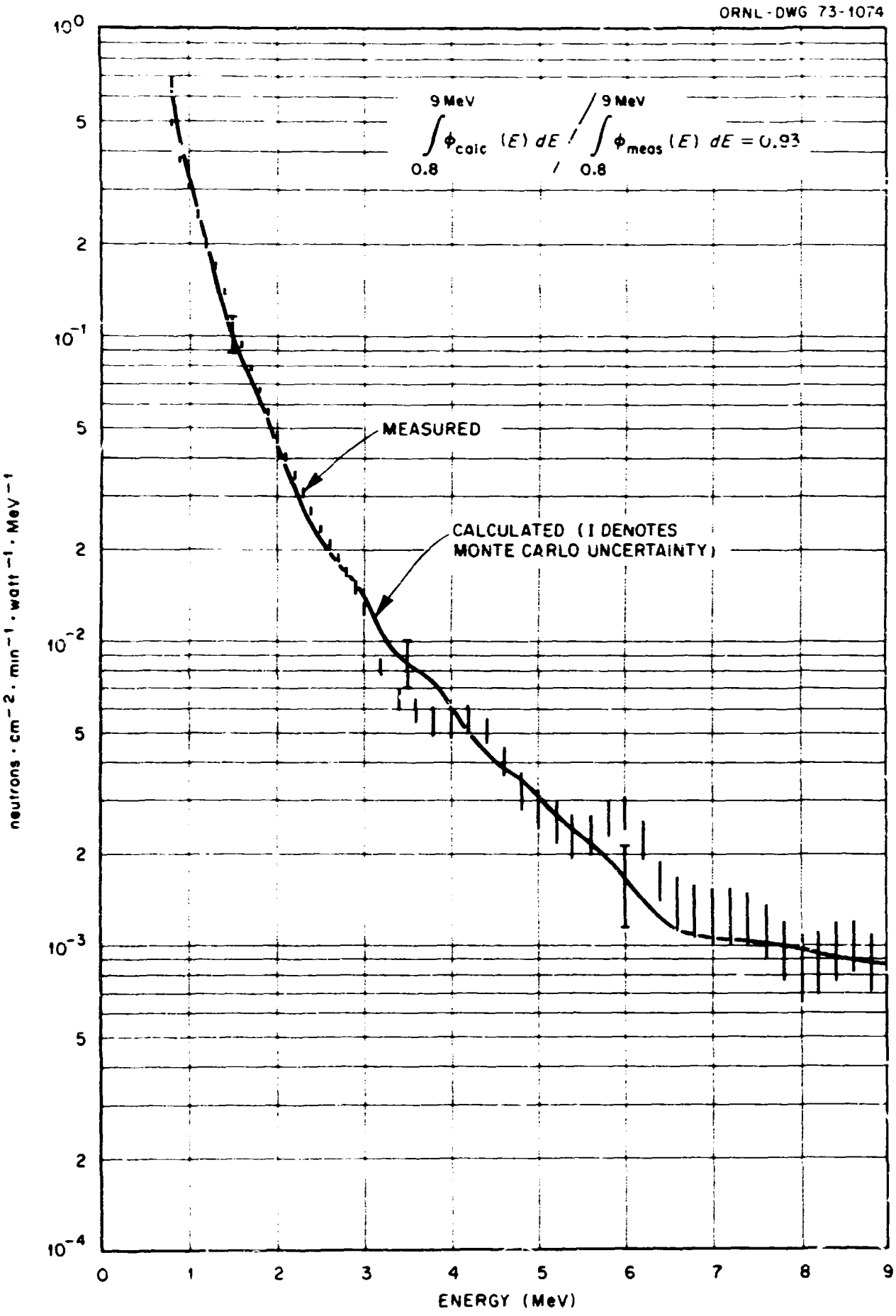

Fig. 13. Comparison of Calculated and Measured SPectra Above 0.8 MeV at 15 Degrees Behind 12 in. of Iron. Calculations used the MAT 4180-Mod. 1 set.

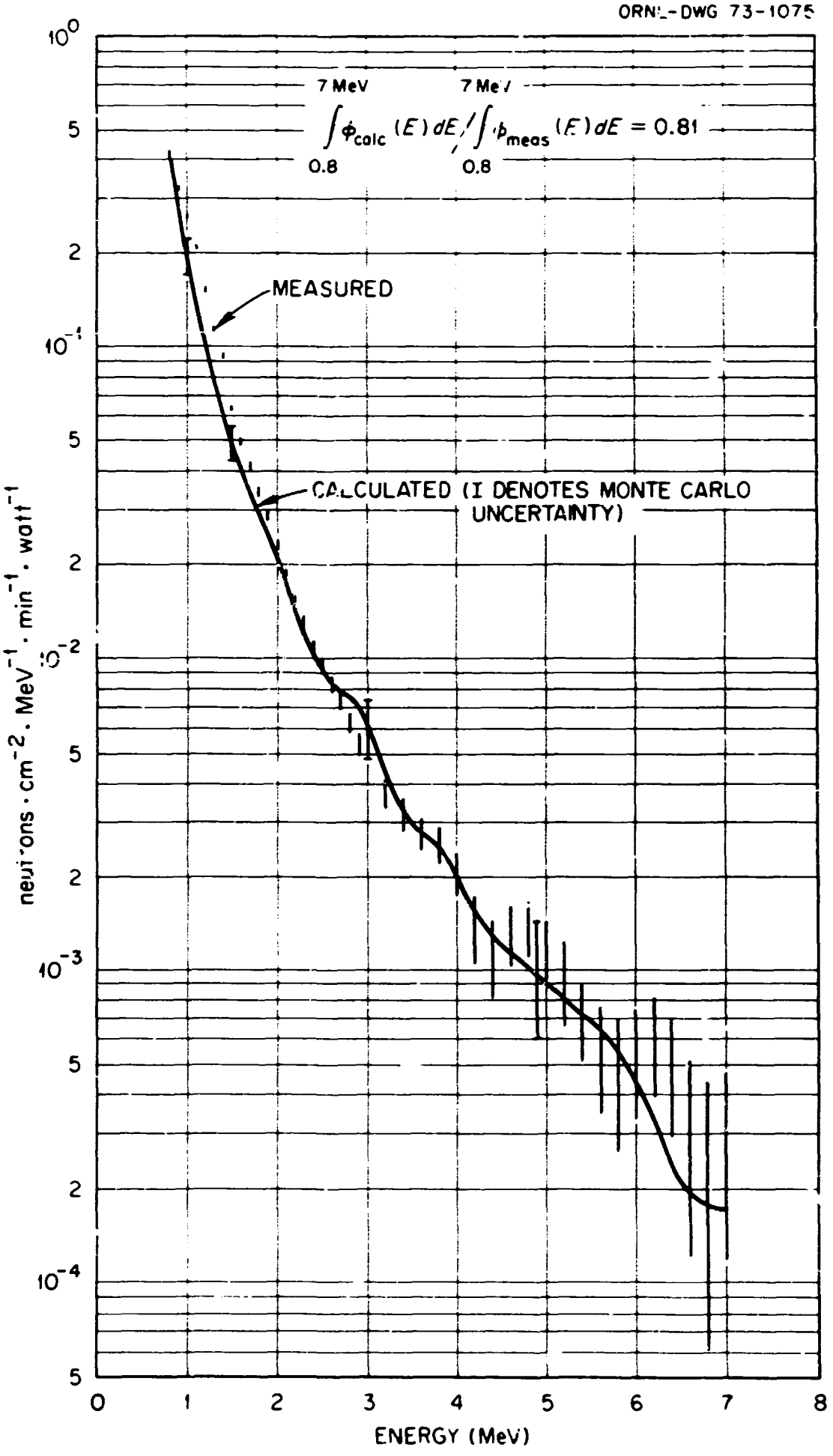

Fig. 14. Comparison of Calcualted and Measured Spectra Above 0.8 MeV at 45 Degrees Behind 12 in. of Iron. Calculations used the MAT 4180-Mod. 1 set.

The comparisons shown in Table XXXVII indicate that the net effect in this energy region of the various changes in the data sets is small, but that the MAT 4180-Mod. 1 set is slightly superior. Since the calculated total flux at the centerline detector in this energy region is only composed of about 25% uncollided neutrons, this spectrum is not very sensitive to the total cross-section changes in the three sets. The slightly deeper minima in the preliminary set result in slightly higher total fluxes in this energy region than those using the final 4180-Mod. 1 set.

The spectra calculated with the MAT 4180-Mod. 1 set, after smoothing with a constant 10% FWHM resolution function, are compared with the measured spectra in Figs. 15 and 16. Figure 15 shows the centerline comparison. The agreement in shape and absolute magnitude is very good with the exception of the region 60 to 90 keV and, to a lesser extent, the regions centered around 150 keV, 220 keV, and 1.25 MeV. The disagreement in the former region may well be due to uncertainties in the measurement since this energy region represents the lower limit of reliability of the spectrometer system at the time it was used. The disagreement in the latter regions is probably due to errors in the cross-section set used in the calculation; in particular, the set underpredicts fluxes around 1.25 MeV and overpredicts fluxes around 220 keV. Figure 16 shows the comparison off the centerline, and again the agreement is adequate with the exceptions and reservations already noted in Fig. 15. There is now better agreement in the region 60 to 90 keV, but the peak in the vicinity of 80 keV is still overpredicted. The calculations are now a little high in the region 400 to 600 keV, but not distressingly so. It is obvious from these two comparisons that the more important features of the cross-section structure for iron in the region 100 keV to 1 MeV are well represented by the MAT 4180-Mod. 1 data.

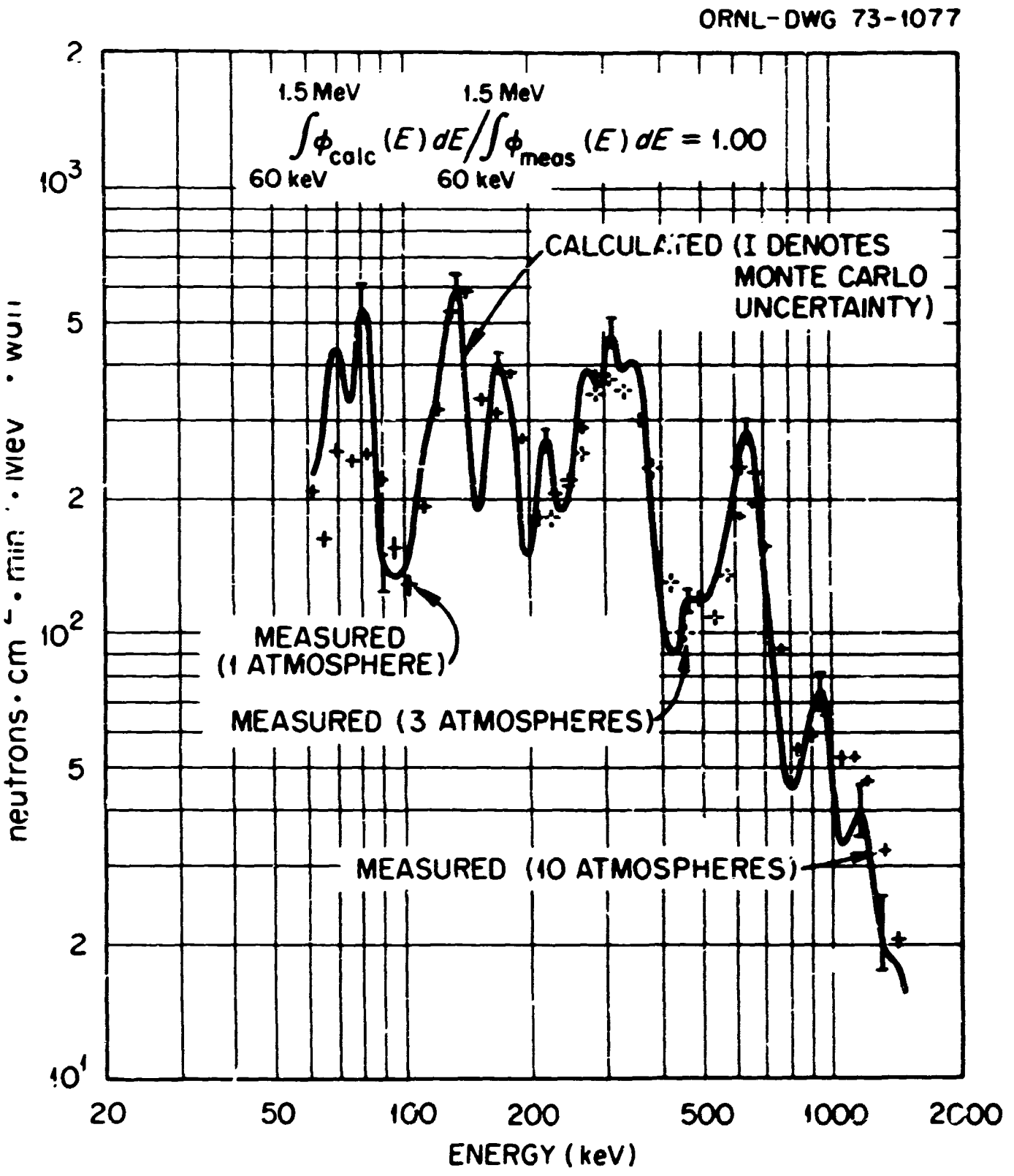

Fig. 15. Comparison of Calculated and Measured Spectra Between 60 keV and 1.5 MeV on the Centerline Behind 12 in. of Iron. Calculations used the MAT 4180-Mod. 1 set.

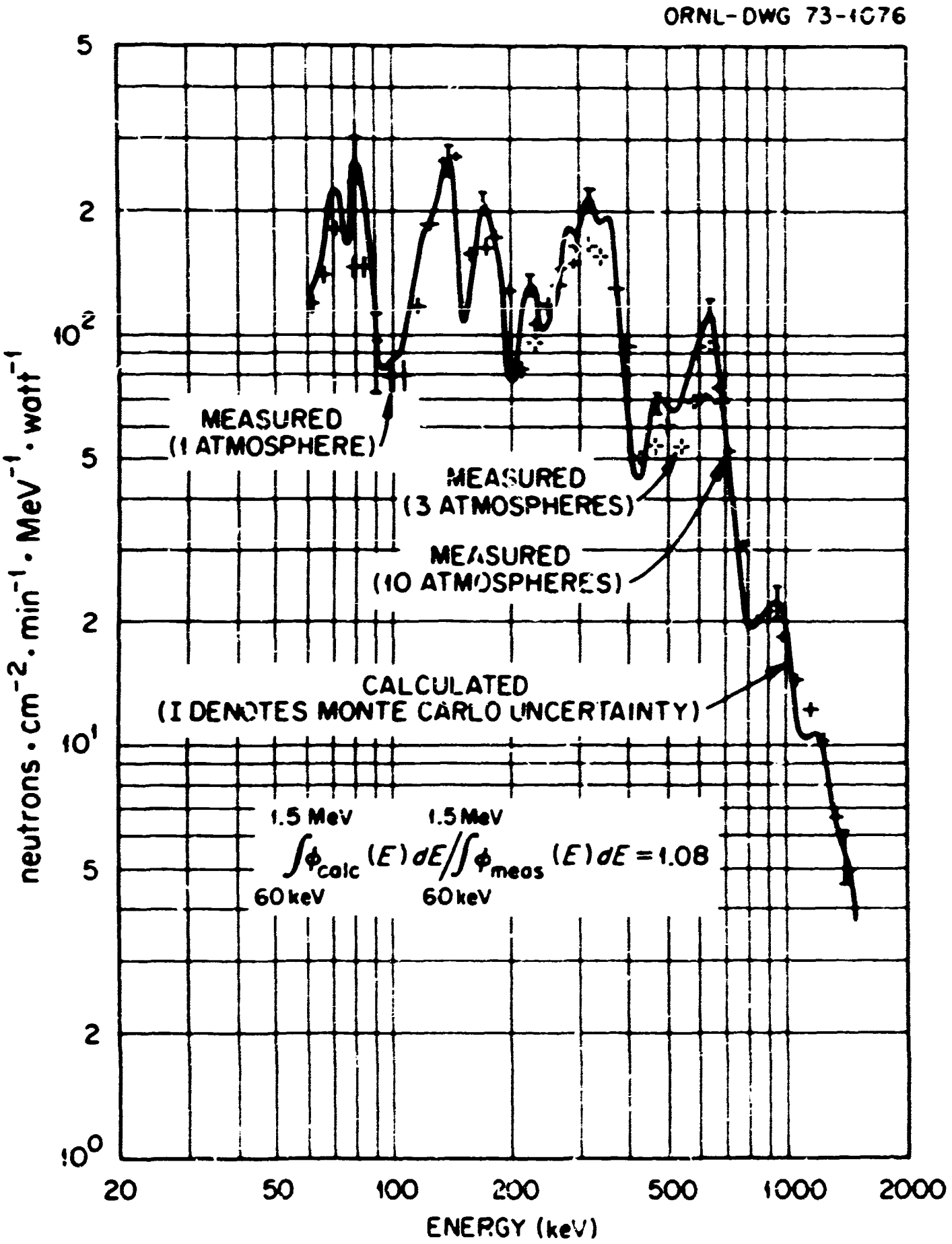

Fig. 16. Comparison of Calculated and Measured Spectra Between 60 keV and 1.5 MeV Off the Centerline Behind 12 in. of Iron. Calculations used the MAT 4180-Mod. 1 set.

Bonner Ball Comparisons Behind 12, 24, and 36 in. of Iron

Calculations of the Bonner ball counting rates behind 12, 24, and 36 in. of iron were made using the MAT 1101, MAT 1124, and MAT 4180-Mod. 1 data sets. Comparisons of the calculated and measured values are shown in Tables XXXVIII-XL. Also included in these tables are the statistical uncertainties in the calculations and the percentages of the calculated centerline counting rates due to uncollided neutrons, both using the MAT 4180-Mod. 1 set. Neither of these numbers changed appreciably for the calculations using the other data sets.

Table XXXVIII. Comparison of Measured and Calculated Bonner Ball Counting Rates Behind 12 in. of Iron in Counts/min/W

Bonner Ball	3-in.			6-in.			10-in.		
	CL	15°	45°	CL	15°	45°	CL	15°	45°
Measured	2.32	0.577	0.411	18.5	3.54	2.39	9.89	1.58	1.04
Calculated (1101)	1.93	0.625	0.433	13.8	3.78	2.56	7.26	1.68	1.11
Calculated (1124)	2.30	0.617	0.430	14.5	3.56	2.44	7.21	1.52	1.01
Calculated (4180-Mod. 1)	2.29	0.541	0.374	16.0	3.49	2.38	8.20	1.64	1.09
Statistical Uncertainty	±0.02	±0.016	±0.011	±0.1	±0.07	±0.05	±0.03	±0.03	±0.02
Calculated Uncollided/ Total	76%	--	--	77%	--	--	77%	--	--
Calculated (1101)/ Meas.	0.83	1.08	1.05	0.75	1.07	1.07	0.73	1.06	1.07
Calculated (1124)/ Meas.	0.99	1.07	1.05	0.78	1.01	1.02	0.73	0.96	0.97
Calculated (4180-Mod. 1)/Meas.	0.99	0.94	0.91	0.87	0.99	1.00	0.83	1.04	1.05

Table XXXIX. Comparison of Measured and Calculated Bonner Ball Counting Rates Behind 24 in. of Iron in Counts/min/W

Bonner Ball	3-in.			6-in.			10-in.		
	CL	15°	45°	CL	15°	45°	CL	15°	45°
Measured	0.604	0.367	0.245	3.49	2.70	1.13	1.40	0.600	0.405
Calculated (1101)	0.430	0.294	0.197	2.33	1.43	0.961	0.913	0.502	0.332
Calculated (1124)	0.613	--	0.257	2.71	--	1.04	0.918	--	0.315
Calculated (4180-Mod 1)	0.613	0.380	0.267	3.24	1.85	1.28	1.21	0.630	0.427
Statistical Uncertainty	±0.040	±0.038	±0.027	±0.13	±0.12	±0.09	±0.03	±0.032	±0.021
Calculated Uncollided/ Total	37%	--	--	42%	--	--	45%	--	--
Calculated (1101)/ Measured	0.71	0.80	0.80	0.67	0.84	0.85	0.65	0.84	0.82
Calculated (1124)/ Measured	1.01	--	1.05	0.78	--	0.92	0.66	--	0.78
Calculated (4180-Mod. 1)/ Measured	1.01	1.04	1.09	0.93	1.09	1.13	0.87	1.05	1.05

Table XL. Comparison of Measured and Calculated Bonner Ball Counting Rates Behind 36 in. of Iron in Counts/min/W

Bonner Ball	3-in.			6-in.			10-in.		
	CL	15°	45°	CL	15°	45°	CL	15°	45°
Measured	0.243	0.181	0.128	1.08	0.700	0.475	0.368	0.227	0.151
Calculated (1101)	0.174	0.150	0.103	0.785	0.635	0.434	0.255	0.193	0.131
Calculated (1124)	0.253	--	0.133	0.900	--	0.451	0.251	--	0.118
Calculated (4180-Mod. 1)	0.228	0.179	0.123	0.985	0.710	0.494	0.318	0.216	0.150
Statistical Uncertainty	±0.029	±0.027	±0.018	±0.037	±0.035	±0.025	±0.009	±0.009	±0.006
Calculated Uncollided/ Total	19%	--	--	25%	--	--	29%	--	--
Calculated (1101)/ Measured	0.72	0.83	0.80	0.73	0.91	0.91	0.69	0.85	0.87
Calculated (1124)/ Measured	1.04	--	1.04	0.83	--	0.95	0.68	--	0.78
Calculated (4180-Mod. 1)/ Measured	0.94	0.99	0.96	0.91	1.01	1.04	0.86	0.95	1.00

The off-centerline comparisons in Tables XXXVIII-XL show the MAT 4180-Mod. 1 set to be superior to the other two, leading to calculated counting rates that agree with the measured values to within about 10% for all the Bonner balls and through all iron thicknesses up to and including 36 in. The other two sets agree almost as well--to within about 20%. However, the centerline comparisons, which are more sensitive to the total cross section since an appreciable fraction of the counting rate is due to uncollided neutrons, offer more striking proof that the MAT 4180-Mod. 1 set is the superior. These calculated counting rates lie within about 15% of the measurements, whereas the counting rates calculated with the other two sets lie within only about 35% of the measurements. The calculated 10-in. Bonner ball centerline counting rates are in general low for all the cross-section sets used. Behind 12 in. of iron, this can be at least partially ascribed to errors in the total cross section in the energy range ~1 to 3 MeV deduced earlier in the NE-213 centerline comparison. Since ~23% of the calculated counting rate on the centerline for the 10-in. Bonner ball is due to neutrons in this energy range (see Appendix) and the NE-213 centerline comparison indicates that the measured fluxes are about 60% higher than the calculated fluxes in this energy range (see Fig. 12), about 23 x 0.6 = 14% of the measured counting rate is absent due to this component alone. The corresponding decrease in the 6-in. Bonner ball centerline counting rate is about 7%, and in the 3-in. Bonner ball centerline counting rate, about 2%. Thus, the errors in the total cross section in the range ~1 to 3 MeV deduced from the NE-213 measurement are sufficient to explain almost all of the centerline discrepancies noted with the Bonner balls behind 12 in. of iron using the 4180-Mod. 1 set. Additional errors are

still present in the other two sets, however. Behind 24 and 36 in. of iron, the contribution of neutrons in this energy range to the calculated 10-in. Bonner ball centerline counting rates is negligible (see Appendix). Thus, errors in the total cross section in the region below ~700 keV are still indicated for the 4180-Mod. 1 set, although these cross sections are more accurate than those in the other two sets.

A comparison of some of the calculated centerline fluxes at the Bonner ball location behind 12 in. of iron using both the MAT 1124 and MAT 4180-Mod. 1 sets is shown in Table XLI.

Table XLI. Comparison of Some of the Calculated Fluxes At the Centerline Bonner Ball Location Behind 12 in. of Iron Using the MAT 1124 and MAT 4180-Mod. 1 Data Sets in Neutrons/cm^2/min/W

Energy Range (keV)	Calculated Flux					
	MAT 1124			MAT 4180-Mod. 1		
	Uncollided	Scattered	Total	Uncollided	Scattered	Total
1587-2590	0.405	0.053	0.458	0.405	0.066	0.471
998-1587	1.00	0.097	1.10	1.00	0.140	1.14
700-998	1.10	0.144	1.24	1.10	0.205	1.31
433-700	1.59	0.381	1.97	1.85	0.538	2.39
250-433	1.69	0.551	2.24	2.42	0.533	2.95
110-250	0.770	0.506	1.28	1.32	0.421	1.74
30-110	0.103	0.227	0.330	0.269	0.166	0.435
10-30	3.14	0.284	3.42	1.69	0.219	1.91
Sum 10-2590	9.80	2.24	12.04	10.06	2.29	12.35

It is to be observed from Table XLI that, although the integral values over the energy region 10 keV-2590 keV are about the same for both cross-section sets, the scattered spectrum is somewhat harder for the MAT 4180-Mod. 1 set. Thus for the Benjamin counter location behind 12 in. of iron (see Table XXXVII), where most of the centerline flux is scattered and of course all the off-centerline flux is scattered, the MAT 4180-Mod. 1 set produces somewhat higher fluxes in the energy region above ~400 keV and somewhat lower fluxes below ~400 keV, relative to those using the MAT 1124 set.

Benjamin Counter Comparisons Behind 12 in. of Stainless Steel

Calculations of the Benjamin counter spectra behind 12 in. of stainless steel were carried out using both the MAT 1124 and the preliminary version of MAT 4180-Mod. 1 cross-section sets for iron. Comparisons of the spectra integrated over the energy interval from 90 keV to 1.3 MeV are shown in Table XLII.

Table XLII. Comparison of Integrated Benjamin Counter Spectra With Calculated Values Behind 12 in. of Stainless Steel in Neutrons/cm^2/min/W

	On the Centerline		Off the Centerline	
	Results	Calc/Meas	Results	Calc/Meas
Measured	117		58.4	
Calculated (4180-Mod. 1, Prel.)	125	1.07	68.0	1.16
Calculated (1124)	98.3	0.84	49.0	0.84

The comparisons shown in Table XLII indicate that the use of the preliminary version of 4180-Mod 1 for iron in the stainless steel leads to calculated fluxes in this energy region which agree somewhat better with the measurements. These fluxes are about 10% high, as they were also behind 12 in. of iron (see Table XXXVII). If the final version of this set had been used, the calculated fluxes would probably be about 5-10% less (again see Table XXXVII), thus producing even better agreement behind the stainless steel. It is perhaps surprising that the total fluxes in this energy region at comparable positions behind the stainless steel average about 72% of those behind the iron, even though the total cross-section structure in the two materials is completely different since the minima in the iron total cross section have been "filled in" by the chromium and nickel in the case of the stainless steel.

The spectra calculated with the preliminary 4180-Mod. 1 set, after smoothing with a constant 10% FWHM resolution function, are compared with the measured spectra in Figs. 17 and 18. In Fig. 17, the centerline comparison is shown for which the calculated uncollided contribution is 6%, and in Fig. 18 the off-centerline comparison is shown. Basically, the disagreements occur in the same regions behind the stainless steel as behind the iron, but in general the disagreements are somewhat magnified. Slight overpredictions are still made in the region around 500 keV. The disagreements centered sharply around 150 and 220 keV behind the iron are now broader behind the stainless steel, extending from 125 to 150 keV for the former region and from 160 to 270 keV for the latter region. Since in one region the calculations are high and in the other low, there is little net effect in the flux integrated over both these regions, but errors in

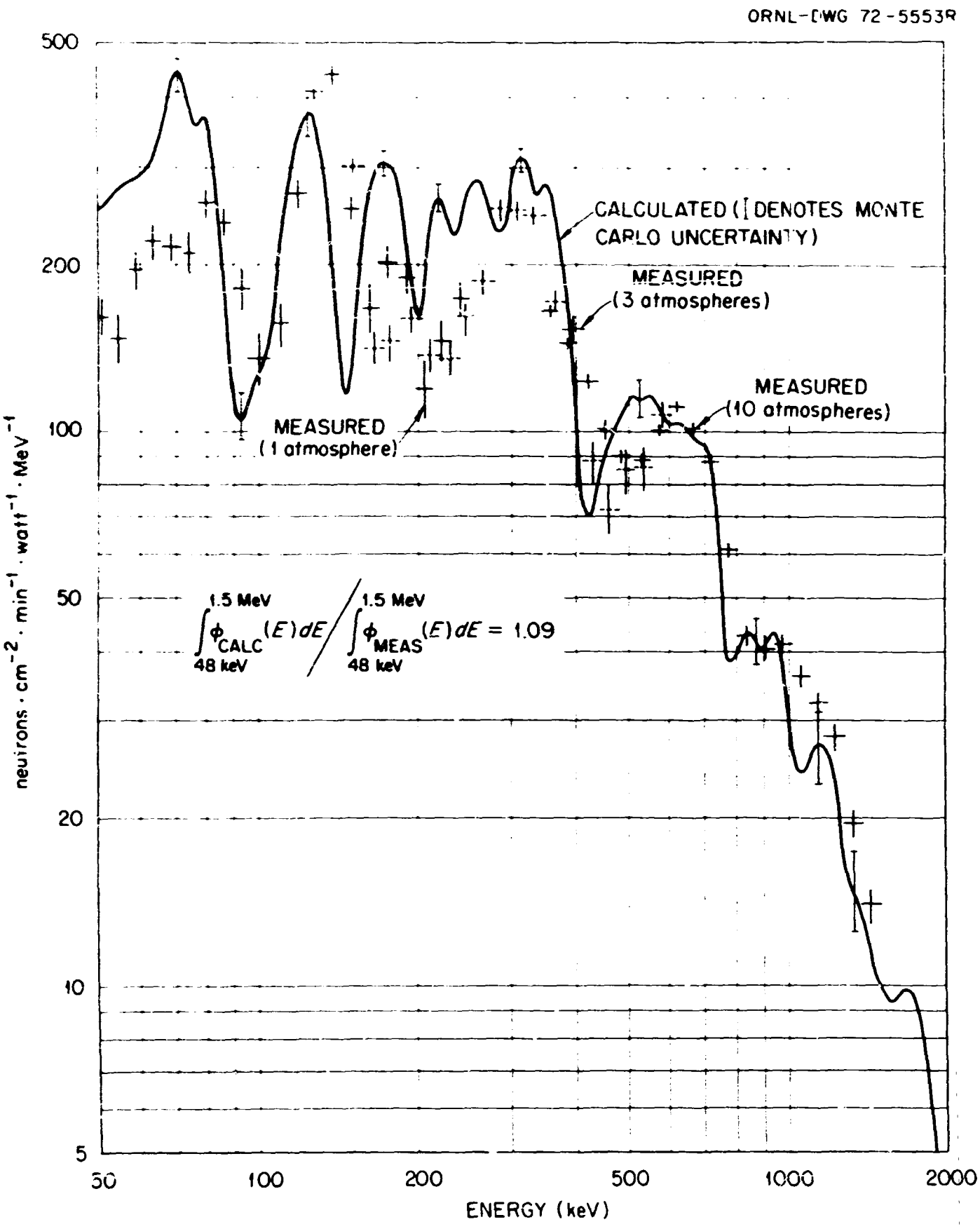

Fig. 17. Comparison of Calculated and Measured Spectra Between 48 keV nd 1.5 MeV on the Centerline Behind 12 in. of Stainless Steel. Calculations sed the preliminary version of the MAT 4180-Mod. 1 set for the iron component.

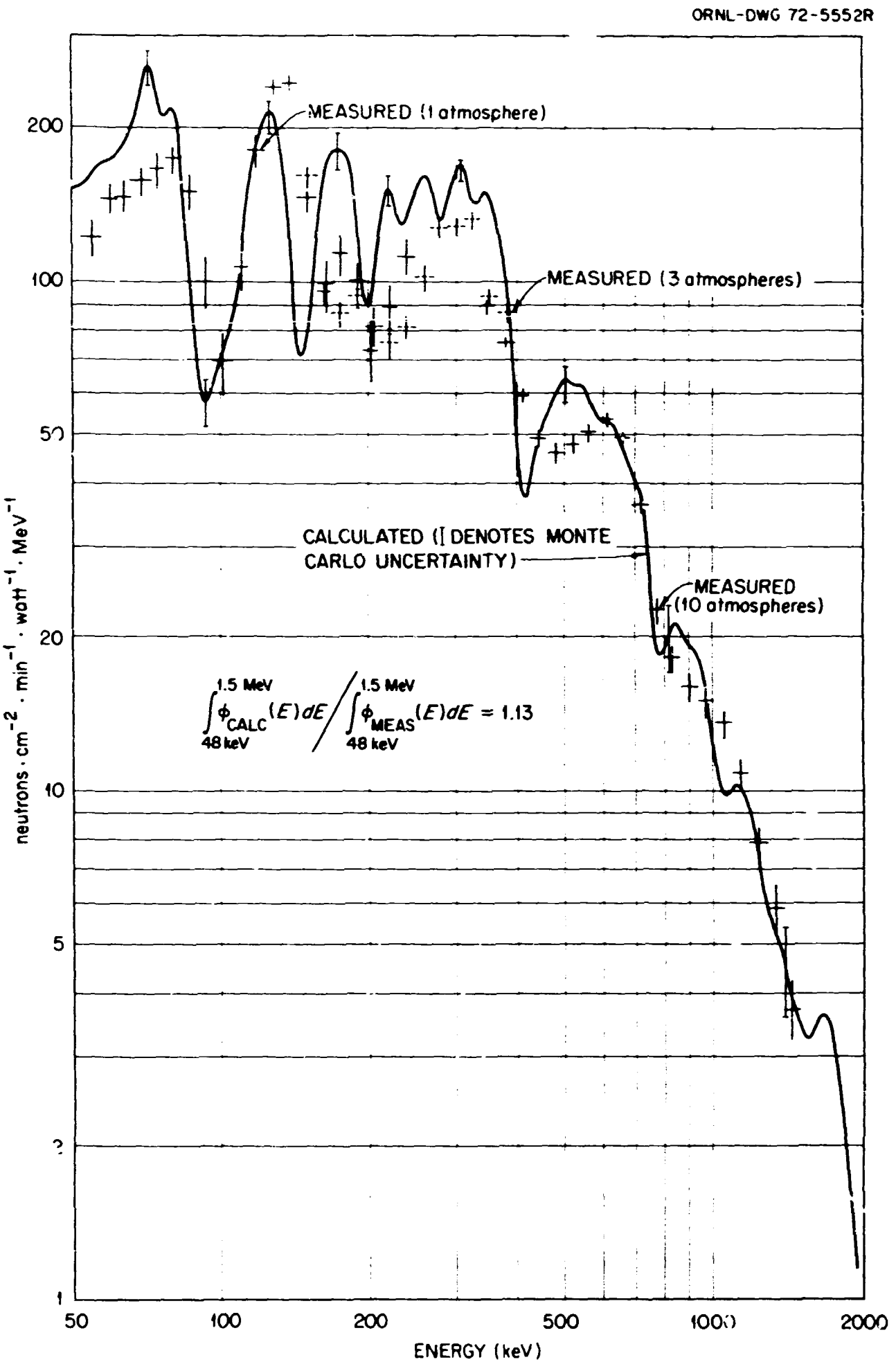

Fig. 18. Comparison of Calculated and Measured Spectra Between 48 keV and 1.5 MeV Off the Centerline Behind 12 in. of Stainless Steel. Calculations used the preliminary version of the MAT 4180-Mod. 1 set for the iron component.

the cross-section set affecting neutrons in at least the higher energy region are nonetheless apparent (correcting the errors affecting neutrons in the higher region alone may also produce agreement in the lower region because of differences in the transport to lower energies). Some of the disagreement in these regions would probably have been reduced somewhat if the final 4180-Mod. 1 set had been used in these calculations.

Bonner Ball Comparisons Behind 12 in. of Stainless Steel

Calculations of the Bonner ball counting rates behind 12 in. of stainless steel were performed with both the MAT 1124 and preliminary version of the MAT 4180-Mod. 1 sets for the iron component. Comparisons of the resulting counting rates are shown in Table XLIII. Also shown are the statistics and uncollided centerline contributions from the calculations using the preliminary 4180-Mod. 1 iron set.

The comparisons shown in Table XLIII again favor the preliminary 4180-Mod. 1 set. The off-centerline agreement using this set is to within about 5%, whereas for the MAT 1124 set the agreement is only to about 20%, with the 10-in. Bonner ball comparison being the worst. For the centerline comparisons, neither set does an altogether satisfactory job, but the preliminary set is clearly superior, yielding counting rates within 25% of the measurements while the MAT 1124 set is only accurate to within 40%. Since over 50% of the calculated centerline counting rate for the 10-in. ball arises from neutrons above 0.7 MeV (see Appendix), and over 50% of the total counting rate is due to uncollided neutrons, it seems logical that there exist errors in the total cross section in this energy range which involve the chromium and nickel evaluations, as well as the iron set. Indeed, the total cross-section minima in chromium and nickel have not

Table XLIII. Comparison of Measured and Calculated Bonner Ball Counting Rates Behind 12 in. of Stainless Steel in Counts/min/W

Bonner Ball	3-in.			6-in.			10-in.		
	CL	15°	45°	CL	15°	45°	CL	15°	45°
Measured	0.783	0.496	0.327	5.97	2.74	1.77	3.51	1.28	0.797
Calculated (1124)	0.589	0.483	0.305	3.78	2.40	1.48	2.18	1.03	0.616
Calculated (4180-Mod. 1, Prel.)	0.689	0.508	0.324	4.80	2.79	1.76	2.66	1.21	0.743
Statistical Uncertainty	±0.016	±0.015	±0.010	±0.06	±0.06	±0.04	±0.03	±0.03	±0.015
Calculated Uncollided/ Total	23%	--	--	39%	--	--	52%	--	--
Calculated (1124)/ Meas.	0.75	0.97	0.93	0.63	0.88	0.84	0.62	0.80	0.77
Calculated (4180)-Mod. 1, Prel.)/ Meas.	0.88	1.02	0.99	0.80	1.02	1.00	0.76	0.95	0.93

received nearly the interest or attention in the past that those in iron have, and for stainless steel they are of comparable importance. Comparisons of the measured Bonner ball counting rates behind 12 in. of stainless steel and 12 in. of iron (Table XXXVIII) illustrate the great significance of the total cross section in the centerline counting rates and the small significance in the off-centerline counting rates. The counting rates on the centerline average about three times higher behind the iron mainly because of the uncollided contribution, whereas off the centerline they average only about 1.25 times higher.

NE-213 Comparison Behind 18 in. of Stainless Steel

A calculation of the NE-213 spectrum behind 18 in. of stainless steel was made using for the iron component the preliminary version of MAT 4180-Mod. 1 for the multigroup set and the final version for the "point" total cross sections. A comparison of the smoothed calculated spectrum with the measurement is shown in Fig. 19. The agreement is in general quite good, although there is probably significance in the slight difference centered around 2.75 MeV. Since at this centerline location only 8% of the neutrons are uncollided, the agreement indicates only that the effects of multiple scattering in the MeV region are treated correctly, but from the discussion already presented, they are not very sensitive to the total cross sections. Errors in the total cross section for stainless steel probably exist in the region above 0.5 MeV, however, because of the disagreement between the calculated and measured 10-in. Bonner ball results on the centerline behind 12 in. of stainless steel, where 52% of the calculated counting rate is due to uncollided neutrons.

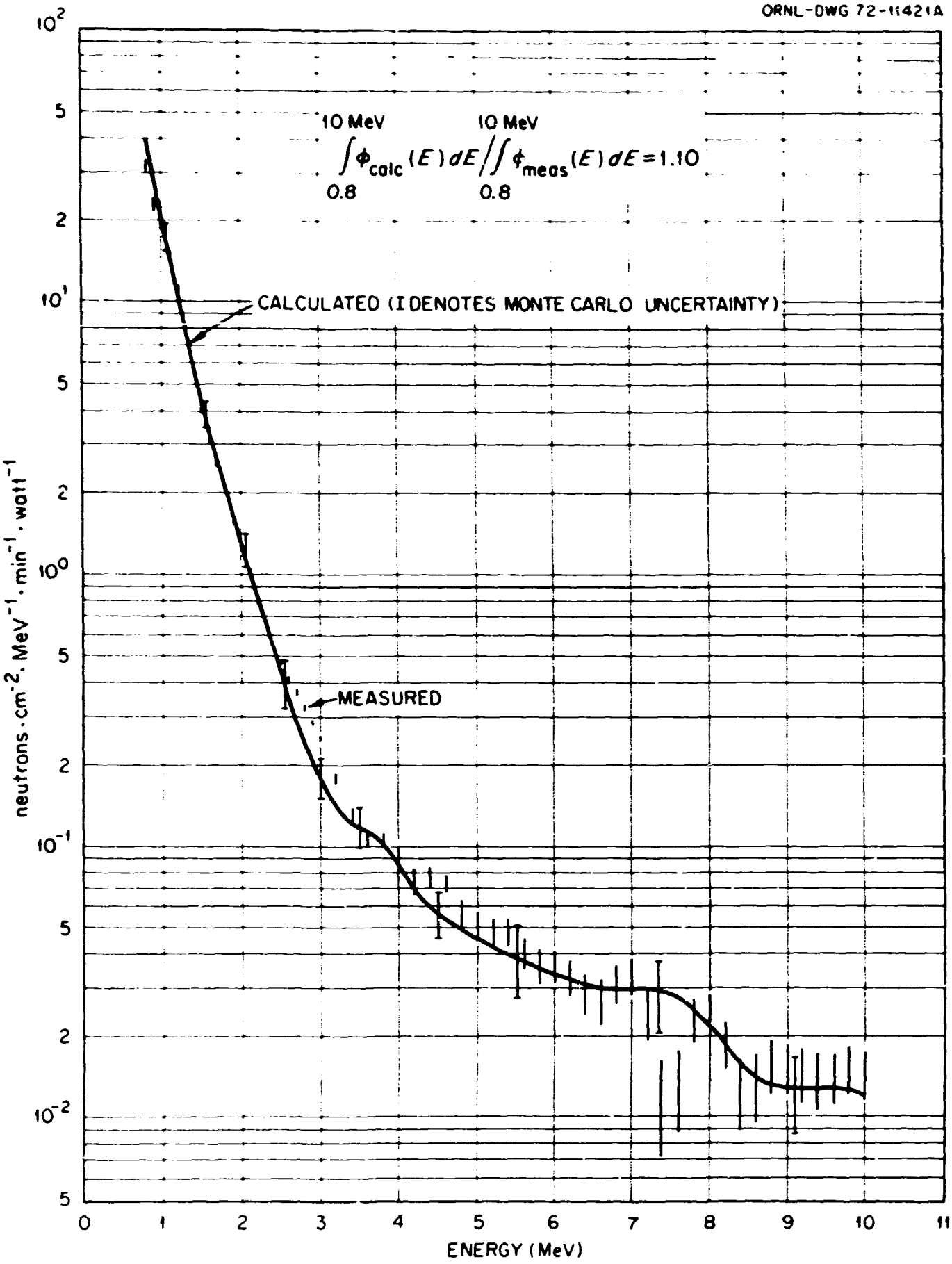

Fig. 19. Comparison of Calculated and Measured Spectra Above 0.8 MeV on the Centerline Behind 18 in. of Stainless Steel. Calculations used the preliminary version of the MAT 4180-Mod. 1 set for the multi-group cross sections and the final version for the point total cross-section iron data.

Benjamin Counter Comparison Behind 18 in. of Stainless Steel

A calculation of the Benjamin counter spectrum behind 18 in. of stainless steel was made using the same combination of preliminary and final versions of MAT 4180-Mod. 1 for iron that was described for the NE-213 calculation. A comparison of the smoothed calculated spectrum with the measurement is shown in Fig. 20. Improvements in the unfolding procedure and the use of the larger collimator, which produces a flux transmitted through 18 in. about 10 times higher than that from the original collimator through 12 in., render these measured spectra more precise than the earlier ones presented, and the reliable data are now believed to extend down to the vicinity of 40 keV. A somewhat improved comparison over the earlier comparisons behind 12 in. of stainless steel is also evident in Fig. 20. The calculations still overpredict the measured fluxes somewhat in the energy regions centered around 220 keV and 180 keV and underpredict the fluxes around 1.1 MeV, 140 keV, and 95 keV. However, below 90 keV there is good agreement down to the vicinity of 40 keV, and in the entire energy region from 300 keV to 1 MeV. The calculated integrated flux in the region covered by the Benjamin counter agrees very well with the measurement. The calculated uncollided contribution at this centerline location is completely negligible (0.4%). Thus, the slab scattered component behind 18 in. of stainless steel is calculated very well for the entire energy range $\sim$40 keV to $\sim$10 MeV, based on the comparisons shown in Figs. 19 and 20.

Bonner Ball Comparisons Behind 18 in. of Stainless Steel

Calculations of the Bonner ball counting rates behind 18 in. of stainless steel were performed using the same combination of "point" and multigroup cross sections based on the MAT 4180-Mod. 1 data set for iron that was described for the NE-213 and Benjamin counter calculations. A comparison of the calculated and measured counting rates is shown in Table XLIV.

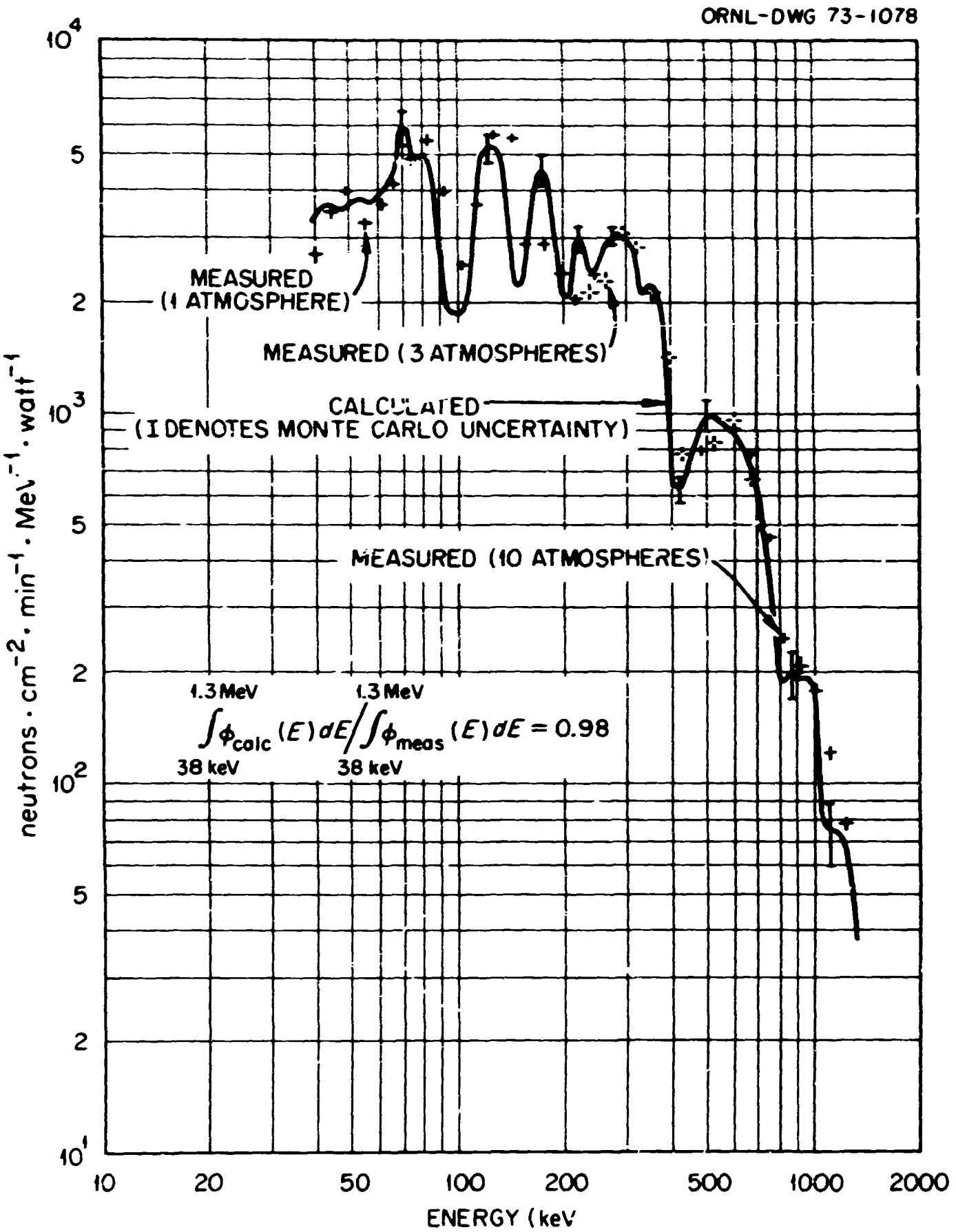

Fig. 20. Comparison of Calculated and Measured Spectra Between 38 keV and 1.3 MeV on the Centerline Behind 18 in. of Stainless Steel. Calculations used the same iron data sets as described for Fig. 19.

Table XLIV. Comparison of Measured and Calculated Bonner Ball Centerline Counting Rates Behind 18 in. of Stainless Steel in Counts/min/W

Bonner Ball	3-in.			6-in.			10-in.		
Distance Behind Slab (in.)	12	72	140	12	72	140	12	72	140
Measured	428	36.6	9.67	2502	218	59.8	1008	83.8	22.4
Calculated	463	33.7	9.16	2844	194	52.4	1074	68.8	17.9
Statistical Uncertainty	±23	±1.7	±0.46	±100	±7	±1.8	±35	±2.3	±0.6
Calculated Uncollided/ Total	0.1%	0.3%	0.6%	0.2%	1.0%	1.8%	0.3%	1.8%	3.3%
Calculated/ Measured	1.08	0.92	0.95	1.14	0.89	0.88	1.07	0.82	0.80

An inspection of Table XLIV shows that the agreement is in general satisfactory except for the 10-in. Bonner ball (and to a less extent, for the 6-in. Bonner ball) at 72 and 140 in. behind the slab, where the calculated counting rates are about 20% low. Since there is good agreement at 12 in. behind the slab, and the uncollided contribution at all three locations is very small, one of two possible conclusions may be drawn. Either the calculated angular distribution of the scattered neutrons is becoming progressively worse as the angle of scatter decreases (i.e., as the centerline detector moves further away), or the measured net counting rate is being overestimated more and more significantly as the detector moves further away. The latter possibility seems to be the more likely one, since the measured background to foreground ratio is increasing with increasing detector distance (see Tables XIV-XVI), and the measured background is an underestimate of the true background. However, the first possibility should not be completely ruled out on this basis alone.

Conclusions

The most significant disagreement between the calculations and the present measurements behind iron leads to the conclusion that the average total cross section in the region ~1 to 3 MeV is too high by about 150 to 250 millibarns in the 4180-Mod. 1 and ENDF/B-III (MAT 1180) evaluations. This conclusion is in agreement with the results of an earlier experiment performed at the TSF.[16] The remaining significant disagreement suggests that the angular distribution of scattering in the region above ~2 MeV is inadequate at least for angles of scattering in the vicinity of 45 degrees. The possibility exists, however, that this disagreement is due to truncated P_0 and P_3 distributions used in the processing code and the disagreement

does not necessarily confirm the presence of errors in the 4180-Mod. 1 evaluation. Less significant disagreements also suggest minor cross-section errors leading to neutrons in the vicinity of 150 keV and 220 keV.

From the comparisons of calculated and measured results behind stainless steel, the above conclusions regarding iron are reinforced. Additional significant errors in the chromium and/or nickel cross sections affecting neutrons in the regions 130 to 250 keV and above ~500 keV also are indicated.

In general, however, there is remarkably good agreement between the calculations using the 4180-Mod. 1 data and the measurements, and the overall conclusion to be drawn is that the 4180-Mod. 1 data set for iron using the Harvey total cross section minima measured at 80 meters from 60 to 800 keV gives good agreement with most of the measurements presented. The use of previous iron evaluations gives significant errors in the calculated transmission of neutrons through thick iron shields. While these good comparisons show that accurate calculations can be performed for up to 36 in. of iron for the configurations used in the experiment, sensitivity studies should be performed to relate the comparisons to design problems where the source spectrum and "detector" response functions may be quite different.

Acknowledgments

The authors wish to acknowledge the efforts of all the personnel at the Tower Shielding Facility for performing the measurements described here, including K. M. Henry, Jr., L. B. Holland, J. L. Hull, J. J. Manning, J. N. Money, and K. M. Freestone, Jr. We also acknowledge the assistance of M. B. Emmett in performing the MORSE calcualtions through 18 in. of stainless steel.

Appendix

The following tables (AI-AVI) present a summary of the relative contribution to the calculated centerline Bonner ball counting rates using the 4180-Mod. 1 data set from various energy ranges of the spectra leaking the slabs. In addition, the relative leakage spectra are also given. It is to be observed that the 6-in. Bonner ball is a good detector for measuring the total flux in the energy range 0.41 eV-10 MeV. The 3-in. ball weights the low energy end more heavily, and the 10-in. ball weights the high energy end more heavily.

Table AVII shows a comparison of the neutron leakage from a 1-meter-radius iron sphere with a point fission source located at the center using 100-group (GAM-II) and 220-group cross sections, both weighted $1/E\sigma_T$ and based on the MAT 4180-Mod. 1 data set for iron. The calculations were performed using ANISN by V. Rado. Besides the interesting group-by-group comparisons, it should also be pointed out that most of the absorption taking place in the sphere occurs at non-thermal energies. Thus, the resonance absorption cross sections play an important role in the transport of neutrons through large thicknesses of iron.

Table A I. Percentage of Calculated Bonner Ball Counting Rates and Epicadmium Fluxes Due to Neutrons in Various Energy Groups Incident on the Bonner Balls on the Centerline in the Free Field†

Bonner Ball	3-in.	6-in.	10-in.	Relative Flux
2.6-10 MeV	2.4	19.0	40.0	28.6
1.0-2.6	5.4	29.7	39.7	27.6
0.7-1.0	1.9	6.7	5.6	4.7
0.43-0.7	2.4	6.7	4.4	4.8
0.25-0.43	2.7	5.3	2.6	3.9
0.11-0.25	3.2	4.6	1.7	3.3
30-110 keV	5.3	5.2	1.5	4.0
10-30	5.2	3.8	1.0	3.2
1.14-10	11.9	6.1	1.3	5.2
0.41-1140 eV	59.6	12.9	2.2	14.7

†Values are for the 4-1/4-in. collimator. There are small differences for the 15-1/4-in. collimator.

Table AII. Percentage of Calculated Bonner Ball Counting Rates and Epicadmium Fluxes Using MAT 4180-Mod. 1 Due to Neutrons in Various Energy Groups Incident on the Bonner Balls on the Centerline Behind 12 in. of Iron†

Bonner Ball	3-in.	6-in.	10-in.	Relative Flux
2.6-10 MeV	0.1	0.6	2.0	1.0
1.0-2.6	3.7	10.5	22.7	12.7
0.7-1.0	5.1	10.7	15.4	10.5
0.43-0.7	13.0	20.1	22.2	19.0
0.25-0.43	21.5	25.6	21.1	23.7
0.11-0.25	17.3	14.5	9.1	13.9
30-110 keV	6.0	3.4	1.6	3.5
10-30	31.7	14.3	5.8	15.3
1.14-10	0.6	0.2	0.1	0.2
0.52-1140 eV	1.0	0.1	0.0	0.2

†The contribution to the detector responses from multiple reflection between the slab and the collimator, including the iron collar, was neglected in preparing this table. For the centerline detector locations, this contribution was of the order of 10%, and hence this omission does not materially alter the significance of the entries appearing in the table.

Table AIII. Percentage of Calculated Bonner Ball Counting Rates and Epicadmium Fluxes Using MAT 4180-Mod. 1 Due to Neutrons in Various Energy Groups Incident on the Bonner Balls on the Centerline Behind 24 in. of Iron†

Bonner Ball	3-in.	6-in.	10-in.	Relative Flux
2.6-10 MeV	0.0	0.0	0.0	0.0
1.0-2.6	0.2	0.7	2.1	0.9
0.7-1.0	1.4	3.9	7.7	3.9
0.43-0.7	6.7	13.7	21.0	13.1
0.25-0.43	17.8	27.5	31.5	26.0
0.11-0.25	21.2	23.2	19.4	22.5
30-110 keV	9.5	7.1	4.7	7.4
10-30	39.1	21.8	13.1	24.8
1.14-10	1.8	0.7	0.3	0.8
0.52-1140 eV	2.3	0.4	0.2	0.6

†The contribution to the detector responses from multiple reflection between the slab and the collimator, including the iron collar, was neglected in preparing this table. For the centerline detector locations, this contribution was of the order of 10%, and hence this omission does not materially alter the significance of the entries appearing in the table.

Table AIV. Percentage of Calculated Bonner Ball Counting Rates and Epicadmium Fluxes Using MAT 4180-Mod. 1 Due to Neutrons in Various Energy Groups Incident on the Bonner Balls on the Centerline Behind 36 in. of Iron†

Bonner Ball	3-in.	6-in.	10-in.	Relative Flux
2.6-10 MeV	0.0	0.0	0.0	0.0
1.0-2.6	0.0	0.1	0.2	0.1
0.7-1.0	0.4	1.2	2.7	1.2
0.43-0.7	2.9	7.3	12.5	6.9
0.25-0.43	12.3	23.2	31.3	21.5
0.11-0.25	20.5	28.2	27.3	26.7
30-110 keV	10.2	9.4	7.1	9.6
10-30	35.6	25.2	16.1	27.1
1.14-10	4.5	2.2	1.2	2.4
0.52-1140 eV	13.6	3.2	1.6	4.5

†The contribution to the detector responses from multiple reflection between the slab and the collimator, including the iron collar, was neglected in preparing this table. For the centerline detector locations, this contribution was of the order of 10%, and hence this omission does not materially alter the significance of the entries appearing in the table.

Table AV. Percentage of Calculated Bonner Ball Counting Rates and Epicadmium Fluxes Using MAT 4180-Mod. 1 Due to Neutrons in Various Energy Groups Incident on the Bonner Balls on the Centerline Behind 12 in. of Stainless Steel†

Bonner Ball	3-in.	6-in.	10-in.	Relative Flux
2.6-10 MeV	0.3	1.4	4.2	2.5
1.0-2.6	6.0	15.6	31.9	19.2
0.7-1.0	7.5	15.1	18.8	14.3
0.43-0.7	10.4	16.2	15.6	14.7
0.25-0.43	18.3	21.2	15.3	19.1
0.11-0.25	18.7	15.4	8.5	14.4
30-110 keV	10.9	6.2	2.6	6.1
10-30	14.0	6.1	2.2	6.3
1.14-10	5.1	1.5	0.5	1.6
0.52-1140 eV	8.8	1.3	0.4	1.8

†The contribution to the detector responses from multiple reflection between the slab and the collimator, including the iron collar, was neglected in preparing this table. For the centerline detector locations, this contribution was of the order of 10%, and hence this omission does not materially alter the significance of the entries appearing in the table.

Table AVI. Percentage of Calculated Bonner Ball Counting Rates and Epicadmium Fluxes Using MAT 4180-Mod. 1 Due to Neutrons in Various Energy Groups Incident on the Bonner Balls on the Centerline Behind 18 in. of Stainless Steel†

Bonner Ball	3-in.	6-in.	10-in.	Relative Flux
2.6-10 MeV	0.0	0.1	0.2	0.1
1.0-2.6	0.5	1.6	5.6	2.2
0.7-1.0	1.3	4.2	8.5	4.1
0.43-0.7	5.0	11.9	18.2	11.2
0.25-0.43	11.9	20.9	24.0	19.4
0.11-0.25	20.0	26.0	22.6	24.8
30-110 keV	16.2	14.0	9.5	14.3
10-30	21.6	14.3	8.2	15.3
1.14-10	7.7	3.4	1.7	3.8
0.52-1140 eV	15.8	3.6	1.5	4.8

†The contribution to the detector responses from multiple reflection between the slab and the collimator, including the iron collar, was neglected in preparing this table. For the centerline detector locations, this contribution was of the order of 10%, and hence this omission does not materially alter the significance of the entries appearing in the table.

Table AVII. Comparison of 220-Group and 100-Group (GAM-II) ANISN Results of Leakage from a 1-Meter-Radius Iron Sphere Arising from a Point Fission Source Located at the Center

ΔE	Groups (220)*	Leakage (220) (neuts/source neut)	Groups (100)*	Leakage (100) (neuts/source neut)	Leakage (220)/Leakage (100)
8-10 MeV	1	5.14(-10)**	5,6,f7	6.75(-10)	0.76
6-8	2	7.13(-10)	f7,8,9,f10	8.42(-10)	0.85
4-6	3,4	1.43(-9)	f10,11-13,f14	1.56(-9)	0.92
3-4	5	3.44(-9)	f14,15,16,f17	3.62(-9)	0.95
2.59-3	6	6.46(-9)	f17,f18	4.10(-9)	1.58
2.231-2.59	7-10,f11	1.20(-8)	f18,19	1.31(-8)	0.92
2.019-2.231	f11	1.32(-8)	20	9.98(-9)	1.32
1.827-2.019	f11,12,13,f14	5.86(-8)	21	2.02(-8)	2.90
1.653-1.827	f14,15-20,f21	1.49(-7)	22	8.25(-8)	1.81
1.496-1.653	f21,22-27,f28	2.64(-7)	23	7.64(-8)	3.46
1.353-1.496	f28,29-35,f36	5.05(-7)	24	2.14(-7)	2.36
1.224-1.353	f36,37-42,f43	1.04(-6)	25	2.72(-7)	3.82
1.108-1.224	f43,44-55,f56	2.01(-6)	26	4.17(-6)	4.82
1.003-1.108	f56,57-63,f64	1.35(-5)	27	3.71(-6)	3.64
0.9072-1.003	f64,65-79,f80	1.42(-4)	28	3.28(-5)	4.33
0.8209-0.9072	f80,81-91,f92	9.37(-5)	29	4.26(-5)	2.20
0.7427-0.8209	f92,93-96,f97	4.55(-5)	30	2.04(-5)	2.23
0.6721-0.7427	f97,98-104,f105	3.67(-4)	31	1.10(-4)	3.34
0.6081-0.6721	f105,106-113,f114	2.62(-3)	32	1.77(-3)	1.48
0.5502-0.6081	f114,115-122,f123	1.95(-3)	33	1.47(-3)	1.33
0.4979-0.5502	f123,124-131,f132	1.16(-3)	34	8.77(-4)	1.32
0.4505-0.4979	f132,133-135,f136	2.22(-3)	35	1.21(-3)	1.83
0.4076-0.4505	f136,137,138,f139	9.84(-4)	36	5.30(-4)	1.86
0.3688-0.4076	f139,140-142,f143	2.86(-3)	37	1.08(-3)	2.65
0.3337-0.3688	f143,144-149,f150	7.86(-3)	38	4.28(-3)	1.84
0.3020-0.3337	f150,151-153,f154	1.48(-2)	39	8.22(-3)	1.80
0.2732-0.3020	f154,155,f156	8.50(-3)	40	4.99(-3)	1.70
0.2237-0.2472	f159,160-162,f163	5.06(-3)	42	3.43(-3)	1.48
0.2024-0.2237	f163,164,165,f166	9.23(-3)	43	5.58(-3)	1.65
0.1832-0.2024	f166,167,f168	5.04(-3)	44	2.43(-3)	2.07
0.1657-0.1832	f168,169-171,f172	1.53(-2)	45	8.99(-3)	1.70
0.1500-0.1657	f172,173,f174	7.07(-3)	46	4.84(-3)	1.46
0.1357-0.1500	f174,175-177,f178	2.05(-2)	47	8.44(-3)	2.43
0.1228-0.1357	f178,179-181,f182	1.27(-2)	48	8.27(-3)	1.54
0.1111-0.1228	f182	7.96(-3)	49	6.40(-3)	1.24
86.52-111.1 keV	f182,183,f184	7.25(-3)	50	5.65(-3)	1.28
67.38-86.52	f184,185-191,f192	2.59(-2)	51	1.48(-2)	1.75
52.48-67.38	f192,f193	7.51(-3)	52	6.20(-3)	1.21
40.87-52.48	f193	4.35(-3)	53	3.78(-3)	1.15
31.83-40.87	f193,f194	2.22(-3)	54	1.76(-3)	1.26
24.79-31.83	f194,195-197,f198	1.94(-2)	55	4.93(-3)	3.94
19.30-24.79	f198,199-201,f202	8.92(-2)	56	8.17(-2)	1.09
15.03-19.30	f202,f203	2.42(-2)	57	2.36(-2)	1.03
11.71-15.03	f203,f204	9.39(-3)	58	1.12(-2)	0.84
9.119-11.71	f204,f205	5.84(-3)	59	4.83(-3)	1.21
7.102-9.119	f205,206,f207	1.21(-3)	60	8.90(-4)	1.36
5.531-7.102	f207,208,f209	1.87(-3)	61	1.92(-3)	0.97
4.307-5.531	f209	3.31(-3)	62	3.51(-3)	0.94
3.700-4.307	f209,210	1.38(-3)	f63	1.58(-3)	0.87
1.160-3.700	211	8.02(-3)	f63,64-67,f68	7.77(-3)	1.03
0.2250-1.160	212,213	2.01(-3)	f68,69-72,f73	4.33(-3)	0.46
0.0880-0.2167	214	2.98(-3)	f73,74-77,f78	2.96(-3)	1.01
24.4-88.0 eV	215	2.43(-3)	f78,79-82,f83	2.57(-3)	0.95
6.79-24.4	216	1.74(-3)	f83,84-87,f88	1.91(-3)	0.91
1.89-6.79	217	1.01(-3)	f88,89-92,f93	1.14(-3)	0.89
0.524-1.89	218	4.27(-4)	f93,94-98,f99	4.58(-4)	0.93
0.000-0.524	219,220	1.32(-4)	f99,100	5.68(-5)	2.32
Totals	1-220	3.60(-1)	5-100	2.67(-1)	1.35

*Group numbers prefixed with an f lie in more than one energy interval ΔE.

**Read as 5.14×10^{-10}, etc.

References

1. B. K. Malaviya, N. N. Kaushal, M. Becker, E. T. Burns, A. Ginsberg, and E. R. Gaerttner, "Experimental and Analytical Studies of Fast Neutron Transport in Iron," Nucl. Sci. Eng. 47, 329 (1972).

2. W. R. Burrus, "Utilization of A Priori Information in the Statistical Interpretation of Measured Distributions," Dissertation, The Ohio State University, ORNL-3743, Oak Ridge National Laboratory (1964).

3. W. R. Burrus and V. V. Verbinski, Proceedings of the Special Session on Fast Neutron Spectroscopy, 1964 Winter Meeting of the American Nuclear Society, San Francisco, California, Shielding Division Report ANS-SD-2, p. 148.

4. P. W. Benjamin, C. D. Kenshall, and A. Brickstock, "The Analysis of Recoil Proton Spectra," AWRE-09/68, Atomic Weapons Research Establishment (1968).

5. T. V. Blosser and R. M. Freestone, Jr., "Development of an Epithermal-Neutron Spectrometer," Neutron Phys. Div. Ann. Prog. Rept. Aug. 1, 1965, ORNL-3858, Vol. 1, Oak Ridge National Laboratory (1965).

6. R. E. Maerker, L. R. Williams, F. R. Mynatt, and N. M. Greene, "Response Functions for Bonner Ball Neutron Detectors," ORNL-TM-3451, Oak Ridge National Laboratory (1971).

7. R. E. Maerker, F. J. Muckenthaler, J. J. Manning, J. L. Hull, J. N. Money, K M. Henry, Jr., and R. M. Freestone, Jr., "Calibration of the Bonner Ball Neutron Detectors Used at the Tower Shielding Facility," ORNL-TM-3465, Oak Ridge National Laboratory (1971).

8. A more complete description of this collimator appears in R. E. Maerker and F. J. Muckenthaler, "The Absolute Neutron Spectrum Emerging Through a 15-1/4-in. Collimator from the TSR-II Reactor at the Tower Shielding Facility," ORNL-TM-4010, Oak Ridge National Laboratory (1972).

9. E. A. Straker, P. N. Stevens, D. C. Irving, and V. R. Cain, "The MORSE Code - A Multigroup Neutron and Gamma-Ray Monte Carlo Transport Code," ORNL-4585, Oak Ridge National Laboratory (1970).

10. D. C. Irving and E. A. Straker, "Evaluation of the Cross Sections of Iron: ENDF/B MAT 1101," ORNL-TM-2891 (ENDF-138), Oak Ridge National Laboratory (1970).

11. S. K. Penny and W. E. Kinney, "A Re-Evaluation of Natural Iron Neutron and Gamma-Ray Production Cross Sections-ENDF/B Material 1124," ORNL-4617 (ENDF-139), Oak Ridge National Laboratory (1971).

12. This set was evaluated by F. G. Perey of Oak Ridge National Laboratory and includes the 80-meter measurements of J. A. Harvey of the total cross section minima for neutron energies between 60 and 800 keV on ORELA.

13. R. Q. Wright, J. L. Lucius, N. M. Greene, and C. W. Craven, Jr., "SUPERTOG: A Program to Generate Fine Group Constants and P_n Scattering Matrices from ENDF/B," ORNL-TM-2679, Oak Ridge National Laboratory (1966).

14. R. E. Maerker, "SDT 11. The ORNL Benchmark Experiment for Neutron Transport Through Iron and Stainless Steel, Part I," ORNL-TM-4222 (ENDF-188), Oak Ridge National Laboratory (1974).

15. R. E. Maerker, F. J. Muckenthaler, R. L. Childs, and M. L. Gritzner, "Final Report on a Benchmark Experiment for Neutron Transport Through Thick Sodium," ORNL-4880, Oak Ridge National Laboratory (1974).

16. R. E. Maerker, "SDT 1. Iron Broomstick Experiment--An Experimental Check of Neutron Total Cross Sections," ORNL-TM-3867 (ENDF-166), Revised, Oak Ridge National Laboratory (1972). For both the present experiment and the SDT 1. experiment, the effect of possible fine structure in the source beam was investigated and found to be small.

17. A. D. Carlson, R. J. Cerbone, and D. F. Willoughby, "Measurement of Neutron Penetration Standards; Volume II, High Resolution Measurements of the Total Neutron Cross Sections of Nitrogen and Iron," GA 9149 (DASA 2289), Gulf General Atomic (1969).

18. S. Cierjacks, et al., "High Resolution Total Neutron Cross Sections Between 0.5 and 50 MeV," KFK 1000, EUR 3963e. EANDC(E)-111(U), Gesellschaft Fur Kernsforschung M.B.H. Karlsruhe (1968).

19. Subsequent to the present measurements and earlier 80-meter ORELA measurements, J. A. Harvey performed 200 meter measurements of the total cross section at ORELA over the approximate energy range of 1 keV to several MeV, using iron samples of up to 12 inches in thickness. F. G. Perey also performed independent transmission measurements at ORELA in good geometry but with poorer resolution than Cerbone, also through iron samples up to 12 in. thick. In the region 1 to 2 MeV the two ORELA measurements are in good agreement, and indeed show deeper minima than those measured by Cerbone. The Harvey 200 meter measurements will be used in ENDF/B-IV, and are described up to 1 MeV in a paper presented at the National Topical Meeting on New Developments in Reactor Physics and Shielding, held on Sept. 12-15, 1972, in Kiamesha Lake, N. Y., in CONF-720901, Book 2, p. 1075 (1972). These new data produce good agreement with the present center-line measurement behind 12 in. of iron up to 2 MeV, but the disagreement between 2 and 3 MeV remains. Further measurements in the latter energy region are still needed.